The development and validation of a novel, parameter-free, modelling strategy for electromembrane processes: Electrodialysis

Jack Ledingham [a,*], Kyra L. Sedransk Campbell [a], Ben in 't Veen [b], Lucas Keyzer [b], Ngai Yin Yip [c,d], Alasdair N. Campbell [a]

[a] Department of Chemical and Biological Engineering, The University of Sheffield, Sheffield S1 4AA, United Kingdom
[b] Shell Global Solutions International B.V.
[c] Department of Earth and Environmental Engineering, Columbia University, New York, NY 10027-6623, United States
[d] Columbia Water Center, Columbia University, New York, 10027-6623, United States

HIGHLIGHTS

- A general and novel circuit-based model of electromembrane processes is presented.
- A fully validated model of conventional electrodialysis is developed.
- Key developments include novel transport number and membrane resistance models.
- Crucially, the model requires no experimental fitting parameters.
- The model's flexibility allows for extensions to include virtually any phenomenon.

GRAPHICAL ABSTRACT
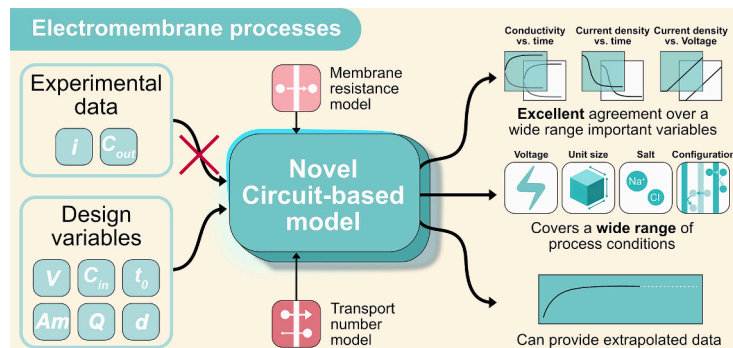
ABSTRACT

As the global water crisis worsens and natural resources of strategic inorganic elements dwindle, the need for efficient and effective salt separation methods is becoming ever more important. Electromembrane processes, and in particular electrodialysis, are emerging as efficient and effective separation technologies that use an electric field to drive the transport of ions against a concentration gradient. Modelling electromembrane processes allows for process design and optimisation, as well as the identification of what technological improvements would have the greatest effect. However, the wide use of empirical fitting parameters in most existing models greatly limits their globality. The presence of complex and confounding phenomena within electromembrane processes greatly exacerbates this. In this work, a novel, circuit-based modelling strategy for electromembrane processes is presented, avoiding the use of any fitting parameters. Conventional electrodialysis is adopted as a case study. The implementation of a novel transport number model and membrane resistance model are crucial for model accuracy over a wide range of process conditions. The model was experimentally validated and showed excellent agreement with experimental data across a range of concentrations and voltages. Consequently, this model will prove to be an excellent tool for researchers and process designers.

1. Introduction

1.1. Background and motivation

As global water scarcity worsens, it is becoming ever more imperative to conserve natural freshwater resources and unlock new sources [1]. Demand for water has increased by an order of magnitude in the last century due to a combination of rapid population growth and societal development [2]. Meanwhile, freshwater resources are rapidly declining due to the discharge of untreated sewage and industrial wastewater [3]. Without rectification, the world will face an estimated water deficit of 40 % by 2030, likely worsened further by climate change [4]. Failure to correct this will result in environmental and humanitarian disasters in the form of ecological collapse and widespread famine. Reusing water in both municipal and industrial settings is the key to water conservation, and brackish water and brine desalination are the most promising pathways to novel freshwater sources.

Electromembrane processes are uniquely positioned as effective and adaptable technologies for the treatment of aqueous ionic solutions [5]. In general, electromembrane processes use an electric field to drive the transport of ions between different streams through ion exchange membranes (IEMs). Membranes are typically either anion selective or cation selective and are layered in a repeating pattern with the solutions flowing between. One repeating unit is known as a 'cell' and when an arbitrary number of cells are placed between two electrodes, the engineering unit of a 'stack' is formed. The electrostatic interactions between the membrane fixed charges and free ions in solution greatly inhibits the transport of like-charged co-ions while promoting the migration of opposite-charged counterions. Anion exchange membranes (AEMs) contain positive fixed charge groups bound to a polymeric backbone which are typically quaternary amine groups. This gives the membrane an overall positive charge which theoretically only permits the transfer of anions. The positive charge of cation exchange membranes (CEMs) typically results from fixed sulfonate or carboxylate groups and thus are selective towards cations.

The quintessential electromembrane process is electrodialysis (ED) [6]. In ED, a unit cell is composed of one AEM and one CEM, with two separate solutions flowing between: a diluate and a concentrate. An electric field is imposed tangentially to the flow by electrodes housed in end-compartments. These electrodes are washed by an electrode rinsing solution to carry away electrode reaction products and are separated from the rest of the stack by end cation exchange membranes (eCEM). The electric field drives ion transfer from the diluate channel, through the appropriate IEM and into the concentrate channel (Fig. 1a). They are
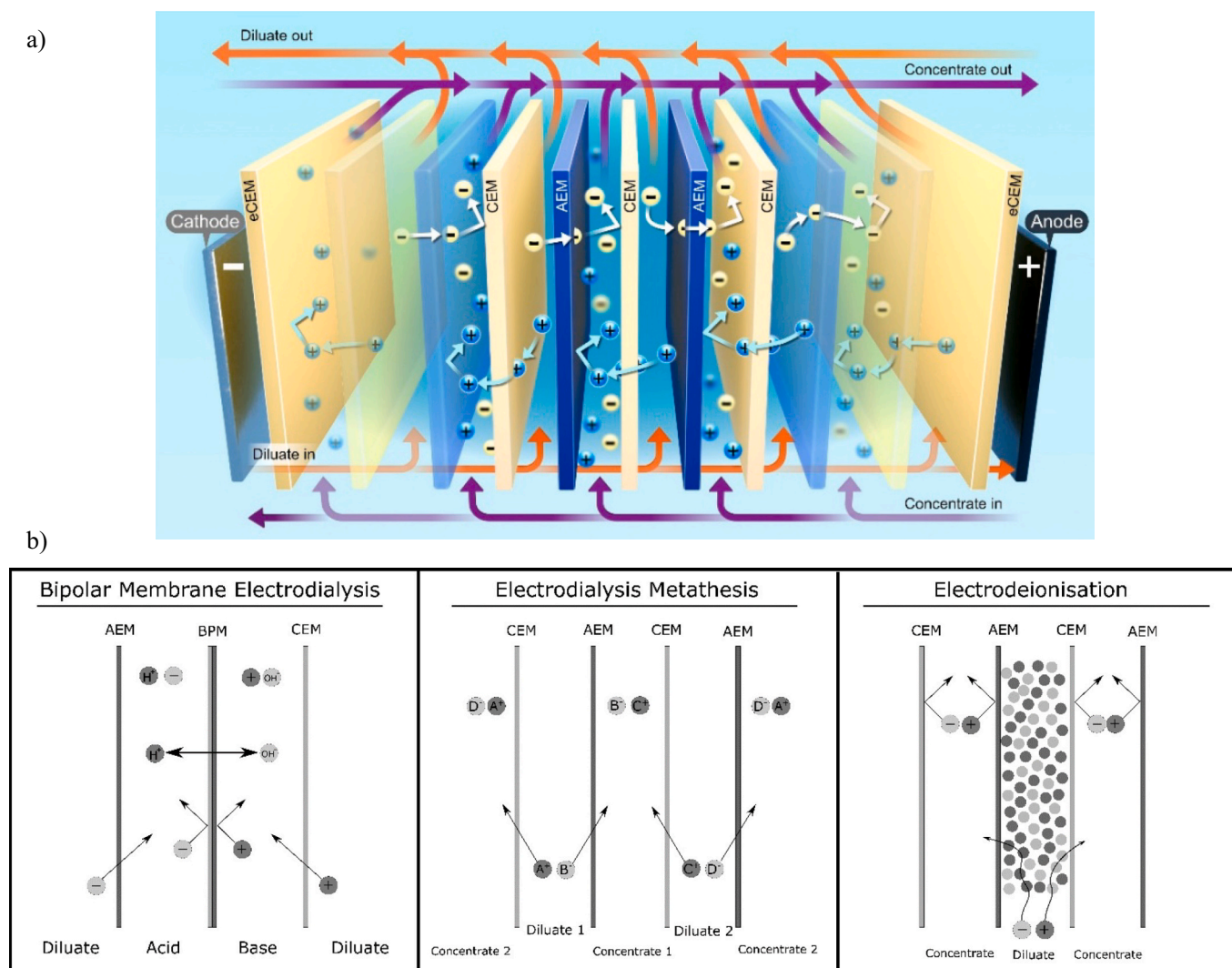

Fig. 1. a) A schematic presentation of ideal transport pathways within ED. b) Schematic representations of other electromembrane processes. Positively charged entities are darker and negatively charged entities are lighter.

theoretically blocked from migrating further by the oppositely charged IEM bounding the other side of the channel. However, an imperfect permselectivity results in some of the ions migrating back to the diluate, wasting energy, and reducing the efficiency. Nevertheless, this process results in an overall transfer of salt from the diluate to the concentrate, effectively separating the salt from a process stream and recovering the separated salts in a second highly concentrated stream.

One of the greatest strengths of electromembrane technologies is the ability to change elements of the unit cell to adapt the functionality to different processes [7]. These modifications can be used to increase the effectiveness of ED under different circumstances or to change the chemical environment of the streams. The primary different forms of electromembrane processes are outlined below, and schematics of some of them can be found in Fig. 1b. Examples of potential and industrially implemented uses of each of these technologies are presented in Table 1.

- **Bipolar membrane electrodialysis (BPMED)**: A bipolar membrane (BPM) consists of an anion exchange layer and cation exchange layer. As such, neither anions nor cations can permeate, only water molecules are able to diffuse in. Once a threshold voltage has been crossed, water splitting occurs at the bipolar junction between the two layers, and the hydroxide and hydronium ions are transported in opposite directions into the adjacent compartments. An additional CEM and AEM are placed adjacent to the BPM, and so three streams are formed: the diluate, acid, and base streams. Consequently, BPMED is useful for adjusting the pH of streams using only electricity or forming concentrated acid and base streams from salt solutions.
- **Electrodialysis Metathesis (EDM)**: The repeating unit of EDM is effectively two conventional ED cells and thus has two diluate and two concentrate streams with two different salts present initially in each of the diluate streams. In EDM, salt pairs are effectively swapped. This can have significant impacts on the properties of the components of each stream, most notably the salt solubility. As such, EDM can function as a very effective pre-treatment step for precipitation or crystallisation reactors without increasing the overall salt concentration.
- **Electrodeionisation (EDI)**: In EDI, ion exchange resins are placed within (typically) the diluate channel to aid transport at low salt concentrations for 'polishing' separations. The resin increases the overall conductivity of the diluate channel and provides a low resistance path for current when salt concentrations are low.

Consequently, EDI translates the benefits of ion adsorption separations into a continuous process.

- **Complexation electrodialysis (CPED):** Complexing agents are added into solutions of a conventional ED process which can be used to change the charge of individual ions by forming complexes. This can drastically alter the selectivity of ED between different like-charged ions by neutralising or increasing the specific charge on certain species.
- **Reverse electrodialysis (RED):** In RED the electrochemical potential difference between two streams of differing concentration drives the diffusion of salts from the diluate to the concentrate, driving electrons around an external electric circuit. Generator plants could be placed at river estuaries, utilising the difference in salinity and electrochemical potential between the river water and seawater to generate electricity.
- **Electromembrane reactors (EMR):** An EMR stack is different to all previous processes mentioned in that the electrodes form part of the repeating unit. Membranes are also used to segregate different flows, which can be either gaseous or liquid solutions. Typical examples of EMR are the chlor-alkali process, where sodium chloride solutions are reacted into sodium hydroxide and chlorine gas, and CO_2 electrolysis where gaseous CO_2 is reduced to useful feedstock chemicals such as ethylene.

At present, reverse osmosis (RO) and nanofiltration (NF) dominate commercial membrane separations due to their maturity and reliability [28] and are a direct competitor to ED for desalination processes. However, there are many inherent advantages that all electromembrane processes, and especially ED, have over RO arising from their fundamental principles and design. A lot of inherent safety concerns are removed by operating ED at ambient pressure rather than the very high pressures required for RO and NF. Membrane fouling is much lower in ED because the salt is transported perpendicular to the direction of flow rather than in RO and NF where the membrane acts as a dead-end filter where foulants are brought to the membrane surface. A greater membrane lifespan, higher recovery ratio, and greater controllability result from the transfer of the minority species (the salt) instead of the majority species (the solvent). The tunability of electromembrane processes are a crucial benefit, where the transport rate is directly controlled by the applied voltage. This makes startup times very low, and process control much easier. Further, the unit size of ED may be reduced by operating at a higher voltage, making it attractive when using expensive membranes or in locations where space comes at a premium. The similarity of electromembrane processes as well as its modularity allows for the reuse of components (membranes, electrodes, housings) for completely different applications.

Current research into electromembrane processes principally focuses on proof-of-concept studies for novel applications [29]. However, very few of these can be implemented at industrial scale due to uncertain performance at this scale and significant uncertainties around process economics. This is, in part, due to the lack of reliable and scalable models that can traverse scales from lab to industry. Therefore, to bridge this gap between the promising research and industrial implementation, process modelling and optimisation is vital. Furthermore, an accurate and general model of electromembrane processes would be able to indicate areas of most beneficial to technological advancement, helping to direct future research and provide a boon for industrial development. Hence, in this work a modelling strategy applicable to all electromembrane processes is presented. The desired model should capture macroscopic behaviour during both steady state and batch modes to model industrial processes as well as laboratory experiments. Further, no empirical fitting parameters are to be used to ensure that the model is valid over a wide range of process conditions. This will ensure that process modelling and optimisation over a range of conditions can be accurate.

Conventional ED is the most fundamental electromembrane process,

Table 1
Application examples of electromembrane processes in recent publications.

Technology	Application	Ref
BPMED	Carbon capture solvent regeneration	[8]
	Production of Biohydrogen	[9]
	Copper recovery from electroplating sludge	[10]
	Biomass pretreatment solvent regeneration	[11]
	Treatment and recovery of Salicylic acid wastewater	[12]
EDM	Ammonia wastewater chemical recovery	[13]
	Potassium nitrate synthesis and purification	[14]
	Production of a wide range of ionic liquids	[15]
	Softening nanofiltration brine to prevent scaling	[16]
EDI	Continuous arsenic removal from wastewater	[17]
	Total desalination to produce deionised water	[18]
	Boron removal using selective resins	[19]
	Pineapple juice deacidification	[20]
CPED	selective zinc removal from electroplating wastewater	[21]
	heavy metal removal	[22]
	organic contaminant removal	[22]
RED	LiBr heat engine to convert low grade waste heat to electricity	[23]
	Desalination of oilfield produced waters with concurrent power generation	[24]
	Power generation from natural waters	[25]
EMR	Partial oxidation of organic pollutants	[26]
	Adiponitrile synthesis from acrylonitrile	[27]

and all others mentioned are built on its foundations. Consequently, a valid model of EDI, BPMED or EDM must be built on a phenomenologically robust and adaptable model of ED. As such, the model presented herein will focus directly on ED, but be flexible enough to be expanded to any electromembrane process.

1.2. Modelling strategies for electrodialysis

Modelling of ED, and all electromembrane processes, is especially challenging due to the multitude of concurrent phenomena at the macro, micro, and nano scale which all interact to affect the overall behaviour. A wide range of ED modelling is presented in existing literature, but, in general, all aim to translate the controlled input variables (inlet concentration and applied voltage) into a measurable outlet concentration (or concentration profile) and current density. Important process performance indicators such as the current efficiency and power consumption can then be obtained. Models of ED can broadly be divided into three categories:

1. **Nernst-Planck Models** [30–36]. Here, the Nernst-Planck equation is solved to generate a multi-dimensional concentration field by summing contributions to the overall flux from diffusion, convection, and electromigration [37]:

$$\boldsymbol{J}_i = D_i \nabla C_i + \boldsymbol{u} C_i + \mu_i z_i C_i \nabla \Phi \tag{1}$$

$$\nabla \bullet \boldsymbol{J}_i = 0 \tag{2}$$

Here, J is the overall flux vector of component i, D_i is its diffusivity, C_i its concentration, μ_i its mobility, z_i its charge number, $\boldsymbol{u}$ is the velocity vector, F is the Faraday constant, and Φ is the electric potential. An additional charge condition is required for closure which either comes from assuming electroneutrality (the sum of all charges at a point, including that provided by the membrane, is zero) or implementing the Poisson equation [38]:

$$\sum_i z_i C_i = -\varepsilon_r \varepsilon_0 \nabla^2 \Phi \tag{3}$$

where ε_r and ε_0 are the relative permittivity of the media and the permittivity of free space, respectively. Due to the multitude of coupled partial differential equations, these models are often solved using the finite element method or finite volume method in computational fluid dynamics (CFD) software such as COMSOL Multiphysics, Ansys Fluent, or OpenFOAM. These models can achieve high resolution on a small scale and thus are useful for investigating localised phenomena, such as concentration polarisation, and the effect of a space charge region [39]. However, the small-scale focus results in extrapolation to full-scale process modelling being inefficient, and thus is not appropriate for the desired modelling strategy.

2. **Semi-empirical models** [40–45] take a basis in ED mass transfer theory but simplify equations, only considering necessary variables and lumped empirical parameters. The parameters are then tuned to ensure model predictions fit existing experimental data. A subset of these models are irreversible thermodynamic models [46] which take their basis in thermodynamic relations rather than mass transfer. Semi-empirical models generally capture process behaviour well but require many experiments to be trained initially, and many more to ensure accuracy over a range of conditions. Semi-empirical models also lack globality, meaning models validated on experimental lab-scale systems will not be applicable at industrial scale. Further, the lumping of empirical parameters obfuscates the effect individual phenomena contribute to overall behaviour, limiting insight and inhibiting process improvement. Since a globally valid model is desired, semi-empirical models are not appropriate.

3. **Equivalent Circuit models** [47–57]: The transport of ions perpendicular to the direction of flow in an ED stack is analogous to

electrons moving in a direct current circuit with solutions and membranes comprising resistive elements. Equivalent circuit models use fundamental theories such as Ohm's law and Faraday's first law to link important variables of ion flux, current density, electrical resistance, and voltage. These models are very flexible in terms of what phenomena they include as additional phenomena can be accounted for through contributions to the resistance and a modification to the material balance. As such, they vary widely in their formulation. Consequently, they are an effective compromise between the two aforementioned modelling methods. A high-level view of an ED system may be taken, while also accounting for essentially any small-scale phenomena deemed important. The most common variations in model aspects are:

- Whether a fixed voltage or current is assumed
- Whether a plug flow reactor (PFR) or continuous stirred tank reactor (CSTR) model is used for the channel material balance
- Whether boundary layers adjacent to the membranes are included
- Whether transport by diffusion is considered
- Whether water transport is present
- Whether electrode reactions and end compartment effects are considered,
- How membrane selectivity is represented (perfect, fixed, or a transport number model)

Each of these phenomena introduces additional intermediate confounding variables to the model (Fig. 2). Due to the complexity of the phenomena considered, most existing models in literature contain empirical parameters which are tuned to fit the model to experimental data. As such, there is an incentive to include as many phenomena and empirical parameters as possible as each addition increases the ability to achieve a good fit to experimental data. This is especially true given the confounding nature of the intermediate variables on the few output variables measured. For example, the rate of diffusion, rate of water transport and membrane selectivity are all solely impacted by the inlet concentration and impact only the outlet concentration. They are not impacted by the applied voltage, nor do they impact the current density. Their impacts are brought about through different intermediate variables which are not measured, and thus cannot be isolated in an empirically driven circuit-based model. This has the additional effect of converging the model onto a single specialised system, reducing globality and the insight that can be gained. Although this is not as problematic as for semi-empirical models due to the stronger basis in physical laws, it still greatly limits the translation of models to other systems and full process scale. The only way to avoid this result without the direct measurement of intermediate variables (extremely challenging, if not presently impossible) is to ensure that there are no empirical parameters present in the model.

In circuit-based models, membranes are typically treated as a 'black box', where simplified empirical parameters are used to attempt to mathematically characterise the membrane. This is required due to the complexity of the myriad electrostatic interactions between all charged species within the membrane. For circuit-based models, these need to be simplified to a membrane selectivity and electrical resistance.

A circuit-based model presented by Wright, Shah, and Winter [58] avoids the use of empirical parameters and was validated against both laboratory and industrial scale batch systems. The agreement between the model and experimental data was initially excellent, but tended to diverge as a more extreme difference in concentration between the diluate and concentrate was encountered. One potential reason could be the assumption of perfect permselectivity. Manufacturer data provided a membrane transport numbers (selectivity) of over 90 %, leading to the seemingly reasonable assumption of ideal permselectivity. However, over the course of the experiment, the concentration difference between the diluate and the concentrate grows, increasing the driving force on co-ions in the concentrate to migrate back to the diluate and reduce the current efficiency. Consequently, a more rigorous approach to defining
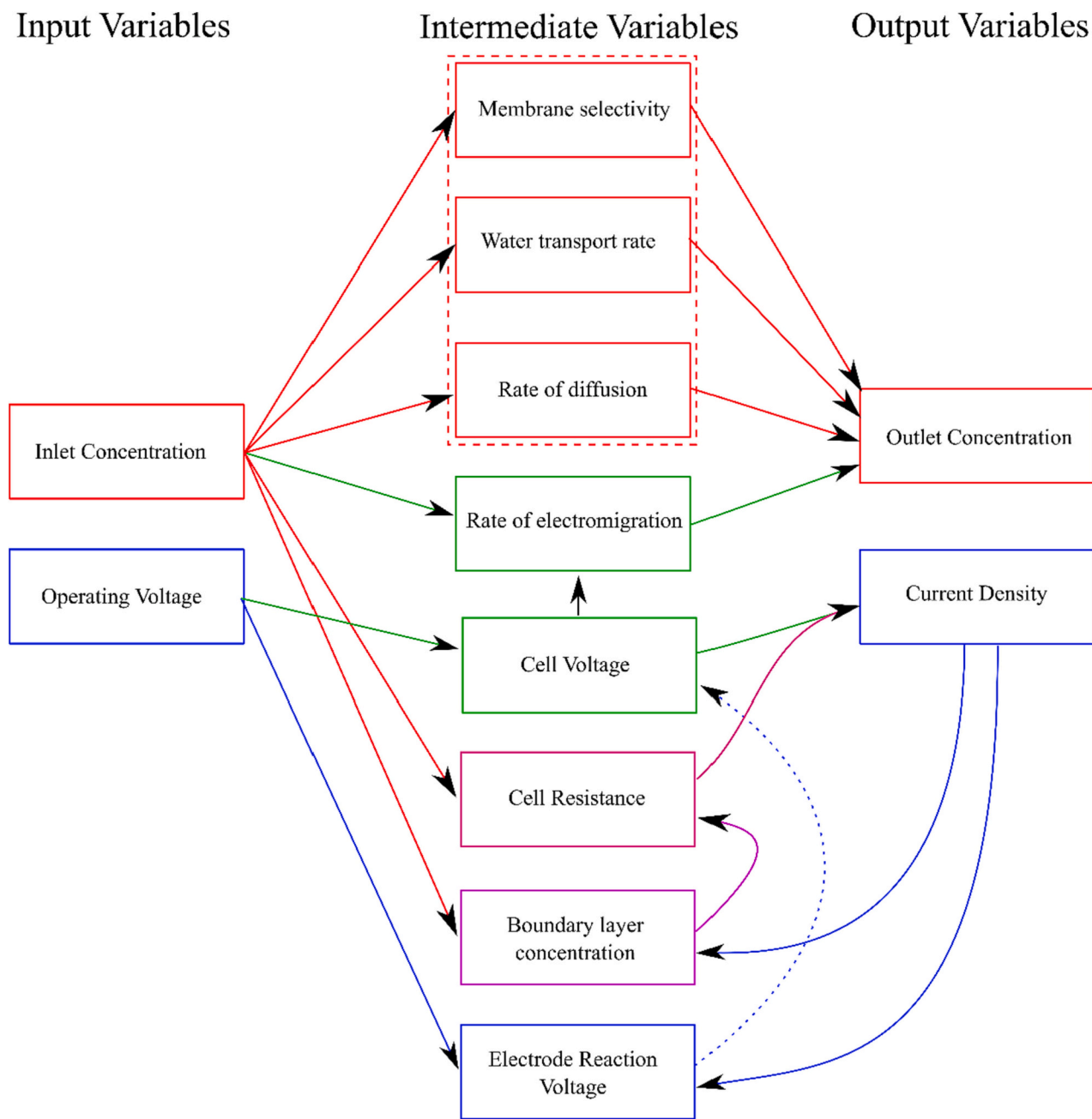
Fig. 2. A flow diagram of common analogous circuit models of ED. The objective of these models is to compute output variables (which may be measured experimentally) from input variables (which are controlled) via intermediate variables which are not measured but represent key phenomena occurring within ED transport processes. The core ED variables are shown in green, the effect of inlet concentration is shown in red, and the effect of the operating voltage is shown in blue. Variables shown in purple are significantly impacted by both the inlet concentration and operating voltage.

membrane selectivity may be required to accurately capture ED behaviour over a wide range of concentration differences. As such, to improve model globality, a membrane transport number model will be implemented in this work.

The membrane electrical resistance is also typically treated as a fixed empirical parameter. Membranes make up approximately 25 % of the cost of a small-scale ED unit [59] and make up a significant proportion of the cost at industrial scale [60]. There is an inherent trade-off between the membrane area required and specific power consumption of an ED stack as they are inversely proportional for a given overall salt transfer rate. Since cost is one of the greatest barriers to widespread ED commercialisation and membrane properties and performance vary widely, there is a great need for accurate representation of the membranes.

Typically, literature models consider the membrane resistance to be fixed. The value is either provided by the membrane manufacturer, measured experimentally, or calculated from the fixed charge concentration. It is desirable to move away from this approach and towards integrating an advanced membrane resistance model such as the one presented by Fan et al. [61].

In this work, a novel equivalent circuit model of conventional ED is presented containing no empirical tuning parameters so as to minimise the inaccurate confounding of variables. This model can straightforwardly be validated against a laboratory scale ED unit and is directly applicable to full industrial scale for process design and optimisation. Notable novel aspects include a transport number model which considers trans-membrane concentration differences, and the adaptation of

a membrane transport model which accounts for electrostatic interactions between fixed and mobile ions. Although derived principally for ED, this modelling strategy may be adapted to any electromembrane process, primarily by altering contributions to the electrical resistance and material balance.

2. Model development

2.1. Model overview

Laboratory experiments of ED (and other electromembrane processes) for proof-of-concept studies are almost exclusively conducted on recirculating batch systems (Fig. 3b). Separate concentrate and diluate reservoirs hold solutions, the concentrations of which vary over time. Conversely, industrial applications of ED are continuous and operate in steady state. The modelling approach presented herein allows for the direct translation of experimentally validated batch model to a full continuous process model. To achieve this, the presented model consists of several layers to achieve this, a flow diagram of which is presented in Fig. 3c.

The inner-most layer is where the Tafel equation and Ohm's law are solved iteratively on a differential volume slice of a cell pair perpendicular to the direction of flow to compute a current density (Fig. 3a). This is then passed to a middle layer and converted to an ion flux using Faraday's first law and a current efficiency model. It is in this layer that the electrical resistance of the differential volume is computed and passed to the inner layer. The ion flux is then integrated across the length of the flow path within the membrane stack in a spatial material balance to determine the outlet conditions. This is sufficient for modelling a continuous process, as the steady-state inlet concentration is fed as an initial condition, and the internal profiles of concentration and resistance, as well as the overall current density and power consumption are computed. However, for batch-mode operation, the inlet conditions are continuously changing. Therefore, an outer layer is present which, for each time step, passes an inlet concentration to the middle layer, returning an outlet concentration. A delayed differential temporal material balance is then used to compute how the reservoir and inlet concentrations vary with time while accounting for the dead time within the pipes.

In this model, it is assumed that water transport and ion diffusion are negligible. These transport phenomena are at least two orders of magnitude smaller than transport by electromigration under normal conditions, and only become important for a low applied voltage [62]. The channel material balance model is that of a PFR, with differential
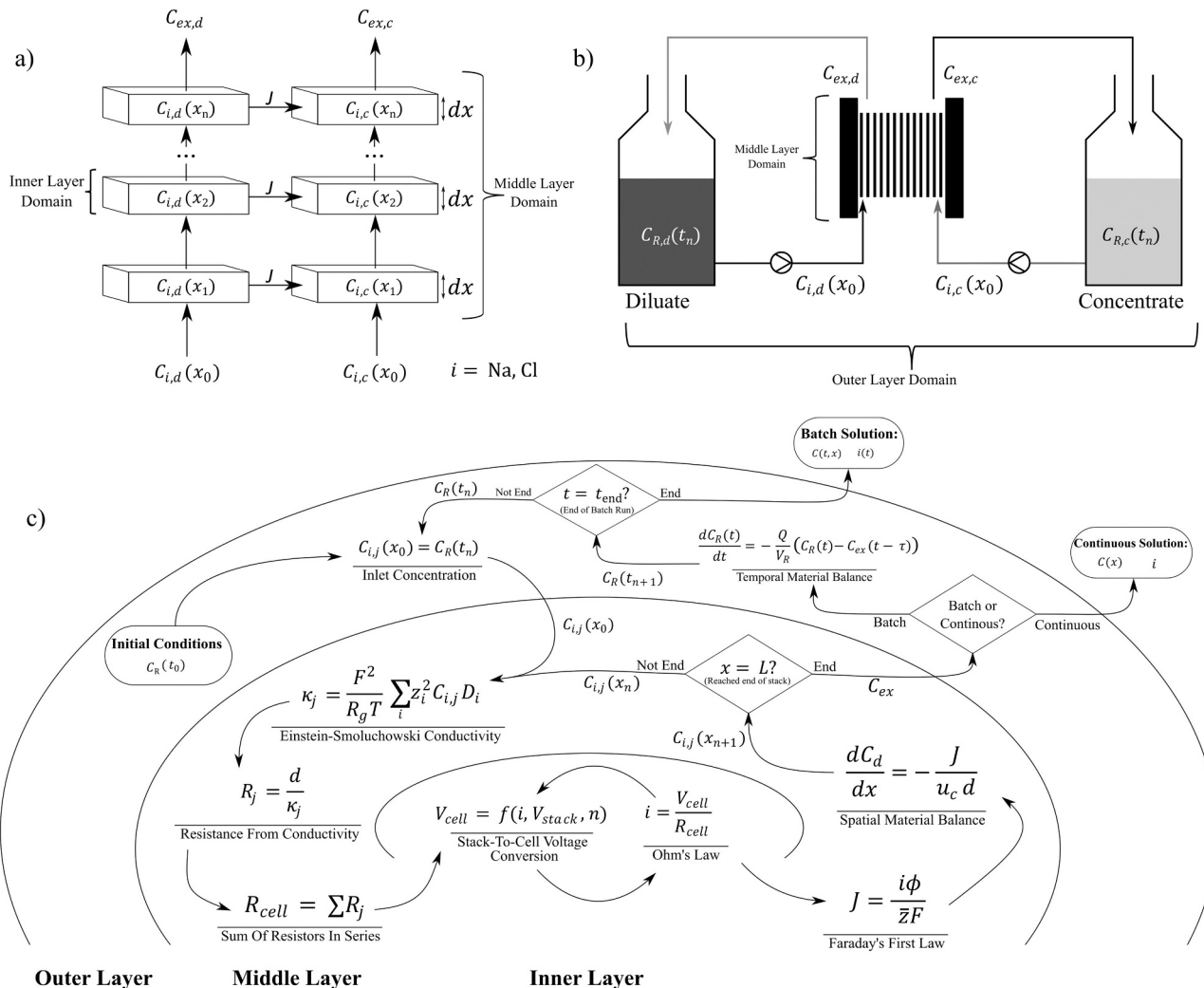

Fig. 3. Schematic representations of various sections of the model. a) A diagram of the differential volumes over which the material balance is conducted (inner layer) and how they are related to find a concentration profile over the path length of the stack (middle layer). b) A schematic of a recirculating batch experiment. Solutions are contained within reservoirs and pumped in a loop though the ED stack and back to the reservoir. The middle layer and outer layer domains are also shown c) A flowchart representation of the overall layered equivalent circuit model. Arrows show the variables passed between different physical laws within the model. The adaptability of the model to both continuous and batch systems can also be seen through the decision point where the outer layer is engaged or not.

material balances solved along the internal flow path. Membrane boundary layers are not considered, as these require empirical models and are only impactful at high voltages and currents approaching the limiting current density (LCD) where this model is not valid. Electrode reactions and end chambers are considered for their contribution to the overall stack voltage. The model primarily considers stack voltage as a fixed input variable rather than the current, as this is what is controlled in typical ED experiments. This model was built and solved in MATLAB version R2022b. The flow of information within the layered approach allows for easy implementation in explicit programming solvers such as MATLAB and Python. However, an implicit solution approach in software such as COMSOL Multiphysics or gPROMS may be preferable. A reformulated model of balanced differential and algebraic equations is presented in an electronic supplementary information document.

2.2. Inner layer: computing current density

In this layer, the cell resistance for the differential volume is passed as an input argument and the associated current density is returned. All other required parameters are unchanging. The current density (i) is computed from the resistance (R_{cell}) and voltage (V_{cell}) of a single repeating cell pair through Ohms law.

$$i = \frac{V_{cell}}{R_{cell}} \tag{4}$$

In order to calculate the voltage of a single cell from the voltage imposed over the whole stack, several potential drops beyond those over the cell pairs must be accounted for. These are the electrode reaction equilibrium potentials (V_{eq}) and overpotentials (η), and the voltage drops over the electrolyte end chambers (V_{ec}). The cell voltage is found by subtracting each of these potential drops from the stack voltage and dividing by the number of cell pairs (n)

$$V_{cell} = \frac{1}{n} \left(V_{stack} - V_{eq} - \eta - V_{ec} \right) \tag{5}$$

The overpotential and end chamber potential drops are functions of the current density. The end chamber resistance is calculated using Ohm's law and a fixed end chamber resistance (R_{ec}) based on the unchanging concentration of the electrode washing solution.

$$V_{ec} = i \left(R_{anolyte} + R_{catholyte} + 2 R_{m,ec} \right) \tag{6}$$

$$R_{anolyte} = R_{catholyte} = \frac{d_{ec}}{\kappa_{m,ec} C_{ec}} \tag{7}$$

Here $R_{m,e}$ is the electrical resistance of the membrane separating the end chambers from the rest of the stack, d_{ec} is the perpendicular distance from the electrode to the end chamber membrane, $\kappa_{m,e}$ is the molar conductivity of the electrolyte, and C_e is the unchanging electrolyte concentration. The overpotential is computed using the Tafel equation [63]

$$\eta = A_a log\left(\frac{i}{i_{0,a}}\right) + A_c log\left(\frac{i}{i_{0,c}}\right) \tag{8}$$

where A and i_0 are empirical parameters found in literature and are dependent on the electrode and electrolytic reactions occurring. The two terms correspond to the overpotentials and the anode and cathode and are summed to compute an overall overpotential. It can be seen in these equations that the overpotential is a function of the current density, but also that the current density is a function of the overpotential. Since only the former is a logarithmic function, this cannot be solved analytically and so must be iterated. The MATLAB function 'fzero' is used iterate over the equations and find a solution. Using this method, the current density for the infinitesimal slice across the stack can be computed and passed to the middle layer.

2.3. Middle layer: electrical resistance and spatial material balance

The middle layer has two primary functionalities: (i) compute the cell resistance to pass to the lower layer, and (ii) to convert the current density returned by the lower layer into an ion flux to be integrated in the spatial material balance.

2.3.1. Cell resistance

An analogous circuit method allows the cell resistance to be calculated by summing the resistances of an arbitrary number of constituents. In this model, four resistive elements are considered: the diluate (R_D), the concentrate (R_C), the AEM (R_{AEM}), and the CEM (R_{CEM}).

2.3.1.1. Electrolyte resistance. The electrolyte resistances of channel j (R_j) is computed from the conductivity of each channel (k_j) and the intermembrane distance (d)

$$R_j = \frac{d}{\kappa_j} \tag{9}$$

The solution conductivity is related to the concentration (C_i), charge number (z_i), and ion mobility (μ_i) of each species, i [37]

$$\kappa_j = F \sum_i |z_i| C_{i,j} \mu_i \tag{10}$$

The ion mobility can be substituted out using the Einstein-Smoluchowski equation [64,65]

$$\mu_i = \frac{F}{R_g T} |z_i| D_i \tag{11}$$

Consequently, an equation is found for the solution conductivity as a function of the ion concentration, charge number and diffusivity

$$\kappa_j = \frac{F^2}{R_g T} \sum_i z_i^2 C_{i,j} D_{i,s} \tag{12}$$

where F is the Faraday constant, R_g is the ideal gas constant, T is the operating temperature, and $D_{i,s}$ is the diffusivity of ion i in solution.

2.3.1.2. Membrane resistance. The resistance of the membranes is determined using a method developed by Fan et al. [61]. In this method, electrostatic interactions between all transported ions (both co-ions and counterions) and fixed charge groups are accounted for and an effective membrane ion diffusivity ($D_{i,m}$) is computed from the diffusivity in free solution.

$$D_{i,m} = D_{i,s} \left(\frac{f_w}{2 - f_w} \right)^2 exp\left(-A z_i^2 \right) \tag{13}$$

Here, f_w is the volume fraction of water in the membrane, and A is a collection of membrane parameters and physical constants, defined as follows

$$A = \frac{\theta e^4 N_A^{2/3}}{16 \pi^4 \varepsilon_m^2 k_B^2 T^2} C_{fix}^{2/3} \tag{14}$$

where θ is a coefficient arising from the summation of infinite vectors (5.48 if fixed charges are assumed to be point charges, refer to the supporting information of [61] for more detail on this), e is the charge of an electron, N_A is the Avogadro constant, ε_m is the permittivity of the membrane matrix, k_B is the Boltzmann constant, and C_{fix} is the membrane fixed charge concentration. The membrane diffusivity can then be used to compute the conductivity (κ_m) of membrane m using the ion mobility and Einstein-Smoluchowski relationship, as in Eq. 12

$$\kappa_m = \frac{F^2}{RT} \sum_i z_i^2 C_{i,m} D_{i,m} \tag{15}$$

To find the counterion and co-ion concentrations inside the membrane ($C_{i,m}$), the Donnan equilibrium equation is utilised with a charge

balance to compute the concentration equilibrium present at the membrane-solution interface [66].

$$\prod_i C_{i,s}^{\nu_i} = \prod_i C_{i,m}^{\nu_i} \tag{16}$$

$$\sum_i C_{i,s} z_i = \sum_i C_{i,m} z_i + z_m C_{fix} \tag{17}$$

Here ν_i is the stoichiometric coefficient (number of ions contributed to the salt) of ion i, $C_{i,s}$ and $C_{i,m}$ are the ion concentrations in the solution and membrane, respectively, and z_m is the charge number of the membrane fixed charges ($+1$ for AEM, -1 for CEM). For two-component salts with a charge of unity (e.g., NaCl), this relation simplifies to the following

$$C_{ct,m} = 0.5 \left(C_{fix} + \sqrt{C_{fix}^2 + \frac{4C_s^2 \gamma_s^2}{\gamma_{an,m} \gamma_{ca,m}}} \right) \tag{18}$$

$$C_{co,m} = C_{fix} - C_{ct,m} \tag{19}$$

where the subscripts ct and co refer to counterions and co-ions, respectively, C_s is the total concentration of solution s, γ_s is the overall salt activity coefficient, and $\gamma_{ca,m}$ and $\gamma_{an,m}$ are the activity coefficients of individual anions and cations inside the membrane, respectively. Since the membrane is adjacent to both solutions, the concentration of an ion within the membrane would be different depending on which solution was considered for the equilibrium. One solution could be to take a simple average of the conductivities computed with either. However, this is not sufficient due to the reciprocal relationship between the conductivity and resistance. Instead, a linear concentration profile between the two membrane-solution interfaces is assumed, and the overall resistance of membrane m (R_m) is found through the integration of this profile. This approach essentially divides the membrane into an infinite number of resistors in series along its width and sums their contributions.

$$R_m = \int_0^{d_m} \frac{dy}{\kappa_m(y)} \tag{20}$$

$$\kappa_m(0) = \kappa_{m1} \quad \kappa_m(d_m) = \kappa_{m2} \tag{21}$$

$$\kappa_m(y) = \kappa_{m1} + (\kappa_{m2} - \kappa_{m1}) \frac{y}{d_m} \tag{22}$$

$$R_m = \frac{d_m \ln \left(\frac{\kappa_{m2}}{\kappa_{m1}} \right)}{\kappa_{m2} - \kappa_{m1}} \tag{23}$$

Here, κ_{m1} and κ_{m2} are the membrane conductivities at the membrane-solution interfaces on either side of the membrane and y is the distance coordinate through the membrane, ranging from zero to the membrane thickness, d_m. Finally, the cell resistance can be found by summing the membrane and electrolyte resistances and passed to the inner layer

$$R_{cell} = R_{AEM} + R_{CEM} + R_C + R_D \tag{24}$$

It is here where the flexibility of the model to be applied to other electromembrane processes is demonstrated. Different electromembrane technologies can be deconstructed into their individual resistive elements which can then be calculated by sub-models and aggregated. For example, an EDI model would have additional contributions to the resistance from the ion exchange resin within the channels. For BPMED, the resistance of the BPM and voltage drops from splitting water at the bipolar junction must be accounted for.

2.3.2. Spatial material balance

Once a current density is returned from the inner layer, a differential spatial material balance can be solved to compute a concentration profile. Faraday's first law is used to convert the current density passed from the inner layer into an overall ion flux (J).

$$J = \frac{i\phi}{\bar{z} F} \tag{25}$$

Here, ϕ is the current efficiency and $\bar{z}$ is half the total charge of the salt (e.g., 1 for NaCl, 2 for CaCl$_2$ and CaO, 6 for Al$_2$(SO$_4$)$_3$). This equation can be extended to allow for consideration of diffusion through the addition of a diffusive flux term (a simplified one would be: $D_m(C_C - C_D)/d_m$). However, the rate of diffusion is typically at least two orders of magnitude lower than the rate of electromigration for most ED applications and its impact is often exaggerated through confounding with back migration. Therefore, diffusion is neglected here.

The current efficiency, ϕ, is the ratio of useful current (resulting in salt transfer from the diluate to the concentrate) to the total current. As such, it accounts for the non-ideal permselectivity of membranes resulting in ions transported from the concentrate back to the diluate. The current efficiency is related to the transport number, $\bar{t}_m$ of each membrane, which is defined as the ratio of the counterion equivalent flux to the total equivalent flux

$$\bar{t}_m = \frac{z_{ct} J_{ct}}{z_{ct} J_{ct} + z_{co} J_{co}} \tag{26}$$

$$\phi = \bar{t}_{CEM} + \bar{t}_{AEM} - 1 \tag{27}$$

A value of $\bar{t}_m$ of unity is representative of perfect permselectivity, whereas a value of 0.5 signifies no discrimination between co-ions and counterions. A value of less than 0.5 would indicate selectivity towards co-ions over counterions.

In ED, it is often assumed that transport numbers are constant (often unity) and not a function of the electrolytic environment. However, this is not realistic, especially for large trans-membrane concentration differences. Herein, a novel transport number model is presented.

Membrane manufacturers often provide an experimental value for the membrane transport number, measured when the trans-membrane concentrations are equal. This value is used in the model and will be considered the 'intrinsic' transport number, $\bar{t}_0$, and has associated counterion and co-ion equivalent fluxes

$$\bar{t}_0 = \frac{z_{ct} J_{ct,0}}{z_{ct} J_{ct,0} + z_{co} J_{co,0}} \tag{28}$$

The migratory flux of ionic species ($J_{m,i}$) is proportional to the ion concentration, according to the Nernst-Planck equation (Eq. 1)

$$\boldsymbol{J}_{m,i} = z_i \, C_i \, \mu_i \nabla \Phi \tag{29}$$

The diffusive flux across membranes for conventional ED is typically a few orders of magnitude below the migratory flux and is thus neglected. Convective flux is not applicable since current is not transported through this method and there is no fluid convection inside the membrane. From this, the ratio between the ion flux at an arbitrary concentration and when the transmembrane concentrations are equal is as follows

$$\frac{J_i}{J_{i,0}} = \frac{C_i}{C_{i,0}} \tag{30}$$

To yield the final model for the transport number of membrane j, Eqs. 28 and 30 are substituted into Eq. 26 along with the fact that $C_{co,0}$ and $C_{ct,0}$ are equal (by definition) to find the final equation:

$$\frac{1}{\bar{t}_m} = 1 + \frac{z_{co} \, C_{co}}{z_{ct} \, C_{ct}} \left(\frac{1}{t_{0,m}} - 1 \right) \tag{31}$$

The current efficiency can then be found by aggregating the transport numbers through Eq. 27 and used in Eq. 25 to find the ion flux. For conventional ED, counterions are transported from the diluate and co-ions from the concentrate, and thus can be substituted appropriately. For a two-component salt such as NaCl, the final transport number

equation becomes:

$$\frac{1}{t_m} = 1 + \frac{C_c}{C_d}\left(\frac{1}{t_{0,m}} - 1\right) \tag{32}$$

As expected, when the concentrate (co-ion) concentration is much larger than the diluate (counterion) concentration ($C_c \gg C_d$), the transport numbers approach zero. In this scenario, the current efficiency becomes negative one as essentially all current is carried by co-ions back-migrating to the diluate. Conversely, when $C_d \gg C_c$, the current efficiency approaches unity. In practice, the transport numbers would not be able to be reduced below 0.5, where the current efficiency would be zero and an equilibrium would be established where the fluxes of co-ions and counterions would be equal and no overall transport would take place.

After the current efficiency and ion flux are calculated, the concentration differential for the concentrate and diluate streams can be computed:

$$\frac{dC_c}{dx} = \frac{J}{u_c\,d} \tag{33}$$

$$\frac{dC_d}{dx} = -\frac{J}{u_c\,d} \tag{34}$$

where u_c is the flow velocity. Only one of these differential equations needs to be solved to find the concentration in one channel, as the other can be found from a material balance. Boundary conditions of the stack inlet concentrations for both streams are passed by the outer layer of the numerical scheme, and integration generates concentration profiles along length of the stack. The function 'ode45' was used to solve the differential equation and compute spatial concentration profiles. Variables of interest such as the voltage over a single cell, current density, overall current efficiency, resistance, and power consumption were then extracted. This model may be directly used as a unit process model or in conjunction with full process simulations in software such as Aspen or gPROMS.

This material balance can be adapted to other electromembrane processes as is required. For BPMED, a series of differential equations is required, one material balance for each species in each channel. This is because there are now multiple different co-ions and counterions, and the current must be split between them. Therefore, accounting for the membrane selectivity between like-charged ions in Eq. 25 is necessary for BPMED and multi-component ED where it is not for conventional ED with only one salt. Reactions taking place in BPMED and EMR are captured through the material balance as well.

An implicit assumption of cell uniformity has been taken throughout this model, principally arising in Eqs. 5, 30, and 33. However, due to the analogous circuit approach of this method, extension to account for inefficiencies such as maldistribution [29] can be accounted for. Cells may be treated individually when computing their resistance with different velocities assigned, and an overall stack resistance computed. This flexibility also allows for potential consideration of a very broad range of phenomena such concentration polarisation and space charge regions.

2.4. Outer layer: temporal material balance

Experimental validation of ED models almost exclusively occurs on recirculating batch units. In these systems, the stack voltage is typically held constant, and salt is transferred from the diluate to concentrate reservoirs. Over time, variables such as the stack inlet concentration, current density, and resistance will change in response to the salt transfer. As such, this model requires an additional temporal material balance as an outer layer to compute how these variables change. This aspect of the model translates the fundamental transport phenomena of the middle layer up to the level of a real batch process. It is not necessary to include this model section for modelling a steady state continuous unit but is essential for a recirculating batch process. This is because in the latter the stack inlet concentration changes over time and so the entire middle and inner layers must be re-solved for each time step.

For a given time, t, the outer layer passes a value of the diluate and concentrate inlet concentrations, C_{d0} and C_{co}, respectively, to the middle layer. For each stream, the outlet concentration (C_{ex}) is returned by the middle layer and used in the temporal material balance on the reservoir concentration (C_R). It is assumed that the reservoirs are well mixed. If pipe dead-time is assumed to be negligible (and thus material transfer from the reservoir to the stack is instantaneous) the inlet concentrations are equal to reservoir concentrations and the temporal material balance for each reservoir is

$$\frac{dC_R}{dt} = -\frac{Q}{V_R}(C_R - C_{ex}) \tag{35}$$

where Q is the volumetric flow rate, and V_r is the reservoir volume. During ED experiments, measurements of pH and conductivity in flow cells are common. The additional dead-volume that tubing and flow cells contribute is often around 0.5 L. This is not negligible compared to the solution reservoirs which typically have a maximum volume of 2 L, and so the dead-time associated cannot be ignored. As such, a time-delayed differential equation is utilised for the temporal material balance. A time delay, τ, is defined as the time taken for a parcel of fluid to travel from the reservoir outlet and back to the reservoir. It is equal to the dead volume divided by the volumetric flow rate. What is essentially happening is that the flow leaving the reservoir is being replaced by the treated fluid which had left the reservoir a time τ in the past. Hence, the delayed differential temporal material balance is as follows.

$$\frac{dC_R(t)}{dt} = -\frac{Q}{V_R}(C_R(t) - C_{ex}(t-\tau)) \tag{36}$$

Initial reservoir concentrations are provided as boundary conditions and the stack exit concentration is computed using the middle layer of the model. Using the MATLAB delayed differential equation solver dde23, temporal reservoir concentration profiles are generated. It should be noted that when comparing experimental data obtained at different positions in the flow circuit, their individual delays must be accounted for. For instance, the current measured at the stack in will not mathematically match with the concentrations present in the reservoir in real time due to the delay between flow exiting the reservoir and entering the stack. The same is true of conductivity measured in flow cells. This will create a mismatch in validation data sets unless it is accounted for, which can be done by shifting the time series experimental data to a standard time or adjusting predicted data to 'real time'. In this work, the latter was performed.

The current density varies along the internal pathlength, but only a single value is measured at a given time. To compute this 'overall' or 'stack' current density, a simple average of the spatially varying current density is sufficient. This is essentially equivalent to summing contributions from an infinite number of resistors in parallel, one for each differential volume. An extension can be added here to consider parasitic currents (also referred to as 'shunt currents') which bypass the membranes and pass through the solutions in the manifolds. This can be done by multiplying the stack current density by an additional efficiency term defined as the ratio of trans-membrane current to total current (sum of trans-membrane current and parasitic current). A resistors-in-parallel approach with resistive elements for the membrane stack and parasitic pathways can be implemented to compute this efficiency [67,68]. However, parasitic currents are typically negligible in ED unless high salt concentrations are present, a scenario where an alternative process such as RO may be preferable. For that reason, parasitic currents are neglected for this model.

3. Model validation

3.1. Validation methods

The inclusion of novel aspects in this model and avoidance of fitting parameters demand experimental validation. All experiments were conducted on a PC BED 1–4 unit (PCCell GmbH) and a PC Cell stack (ED 64004) with ten cell pairs (AEM: PC Acid 60, CEM: PC MV, eCEM: PC MTE). The conductivity and pH of both streams were measured before and after the stack using JUMO CTI-500 inline conductivity probes and JUMO digiLine pH sensors, respectively. The pH has not directly been used in the model validation but was used to ensure that operation was consistently below the limiting current density, where this model would be valid. An SP-300 potentiostat (Biologic) was used to apply a stack voltage and record the current.

Two orthogonal methods were used for validation, both of which used sodium chloride due to its simplicity and prevalence in ED desalination applications. The first of these methods, temporal validation, is a typical recirculating-batch experiment. The initial concentrations of the diluate and concentrate reservoirs are chosen to be equal and the stack voltage is fixed well below the LCD. The solutions are circulated at a constant flow rate and reservoirs are jacketed to maintain a constant temperature.

The other form of validation involves measuring the current and solution conductivities at steady state over a range of voltages and comparing to model predictions. To achieve steady state, the outlet streams from the diluate and concentrate are mixed to 'undo' the separation performed inside the stack and split again before returning to the reservoirs. This ensures that the feed concentrations of both streams remain consistent throughout the experiment. The stack voltage is increased stepwise, holding constant until a steady current is achieved. This steady current and outlet concentration is recorded before the voltage is increased. The use of a potentiostat for these experiments ensures very high accuracy and control over the measured current and applied potential.

The two validation methods undertaken were chosen because they test the validity of the model over a range of concentrations and a range of voltages. These are the most common input variables of ED models and have a large impact on behaviour through confounding phenomena (Fig. 2c). Validity over a wide range of concentrations and voltages without the use of tuning parameters demonstrates that individual confounding phenomena are accurately captured. Membrane properties such as innate current efficiency, thickness, and ion exchange capacity were taken from manufacturer data. These can also be independently measured to guarantee accuracy.

3.2. Temporal experimental validation

Experimental settings and physical parameters for the temporal validation can be found in Table 2. The combination of 10 V stack voltage and 0.05 mol/L NaCl initial reservoir concentration ensured that the current density was below the LCD (independently measured to be ~1.5 A and 18 V) and upper detection limit of the potentiostat (2 A, 36 V). Dead volumes were measured to be 0.41 L and 0.33 L for the concentrate and diluate, respectively.

Experimental and modelling results can be seen in Fig. 4a and b for the solution conductivity and current density, respectively. As expected, over time the conductivity of the diluate decreases and the conductivity of the concentrate increases as salt is transferred from the diluate to the concentrate. It can also be seen that the inlet diluate conductivity is consistently higher than the outlet, showing that salt has been removed from the diluate when passing through the stack. The inlayed graph in Fig. 4a shows the conductivities of the concentrate and diluate very early on in the experiment. Here, the outlet conductivity of the diluate decreases sharply, and before any change in the inlet diluate conductivity is seen. The sharp decrease to outlet diluate conductivity is seen

Table 2
Experimental settings and system parameters used in the temporal validation.

Parameter	Symbol	Value	Unit	Source
Applied Stack Voltage	V_{stack}	10	V	Set by design
Initial reservoir concentration	$C_R(0)$	0.05	mol/L	Set by design
Reservoir volume	V_R	1.0	L	Set by design
Intermembrane distance	d	0.8	mm	Stack Characteristic
Membrane area	A_m	64	cm^2	Stack Characteristic
Recirculation flowrate	Q	20	L/h	Set by design
Temperature	T	297	K	Set by design
Time delay	τ_c, τ_d	59.1, 47.6	s	Measured/Set by design
Diffusivity	D_{Na}, D_{Cl}	1.33, 2.03	$x10^9\ m^2/s$	[69]
Membrane thickness	d_m	0.1	mm	Membrane data from manufacturer
Membrane water fraction	f_w	0.22	–	Membrane data from manufacturer
Fixed charge concentration	C_{fix}	0.8	mol/L	Membrane data from manufacturer
Intrinsic transport number	$\bar{t}_{0,cem}, \bar{t}_{0,aem}$	0.99, 0.96	–	Membrane data from manufacturer

soon after the voltage is activated, and the delay to the response in the inlet diluate conductivity is because of the time taken for the low conductivity solution to flow back to the reservoir, mix with the solution there, and flow out to the conductivity meter. The presence of these delays demonstrates how vital the use of a delayed differential material balance is for these batch ED systems.

The current density is initially high, decreasing over time with a sigmoidal behaviour (Fig. 4b). The decrease in current density is expected due to the increase in the electrical resistance (~20×) while the voltage across a cell only increases slightly (~1.1×, Fig. 4c). The electrical resistance of the solutions is what is primarily driving the increase in overall resistance (Fig. 4d). Since the electrolyte resistance is inversely proportional to the salt concentration (Eqs. 9 & 12), the minimum overall electrolyte resistance (diluate + concentrate) occurs when the two solutions have the same concentration. As salt is transferred from the diluate to the concentrate, the increase in resistance of the diluate is higher than the decrease in the resistance of the concentrate, increasing the overall electrolyte resistance. The slight increase in cell voltage can be explained through Eq. 5. The electrode overpotential is the only quantity that changes as it is a function of the current density. Since this is a logarithmic function (Eq. 8), the overpotential decreases by only 0.95 V despite the fall the current density by over an order of magnitude. This is then further offset by the fixed reaction equilibrium potential and end chamber potential drop, reducing the relative impact of the falling overpotential to only a 13 % increase in cell voltage.

The difference between the diluate inlet and outlet conductivities can be seen in Fig. 4e, with the inlayed graph showing the behaviour very early on. In both the model and experimental results, the conductivity difference spikes initially, remains constant for a short while, drops slightly, and then increases slowly, all in the first 60 s of the experiment. After this, the conductivity difference decreases over the rest of the experiment, ending in a very low value (0.0015 mS/cm). The initial erratic behaviour is a direct result of the delays incurred from the pipe dead time. The original spike occurs because the outlet conductivity falls long before a change in the inlet conductivity is seen. Since the inlet concentration is constant during this time, the outlet concentration is as well. Once the response is detected by the inlet conductivity probe, it takes time for this to be measured by the outlet probe, as they have a relative delay of about ten seconds between them. This is what causes the rest of the odd behaviour. Once again, this demonstrates the
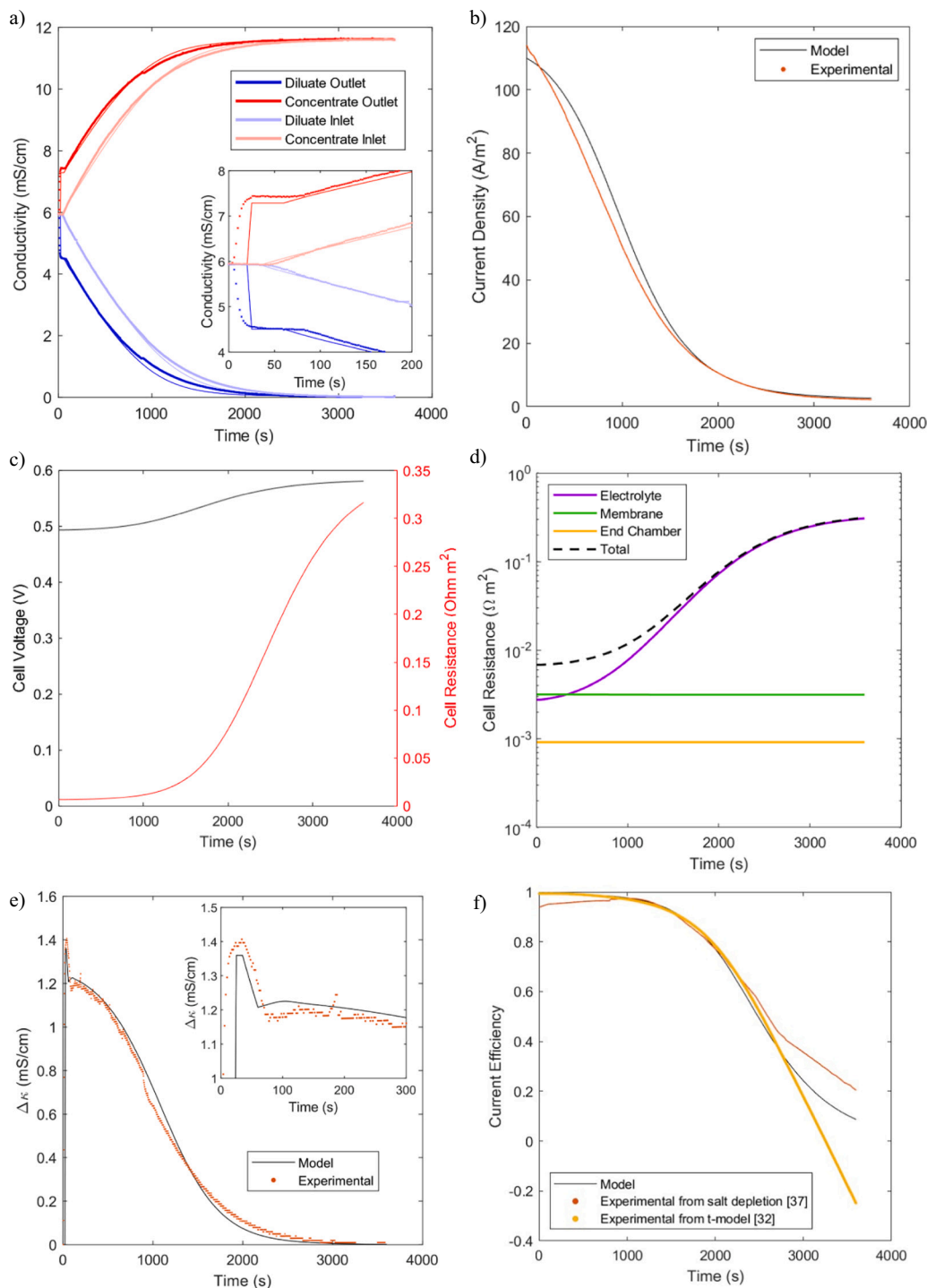
Fig. 4. Experimental and modelling results for temporal experiments. a) Evolution of the experimental and model conductivities over time for the inlet and outlet of diluate and concentrate steams. Model predictions are solid lines and experimental data points are shown as crosses b) The current density evolution over time for both the experimental and model-predicted series. c) A graph showing the evolution of the calculated cell voltage and cell resistance over time. d) A graph showing the constituent electric resistances which comprise the overall stack resistance. It should be noted the y-axis is on a logarithmic scale. e) The time evolution of the difference in conductivity between the inlet and outlet of the diluate stream. f) The calculated current efficiency over the validation experiment, as well as the smoothed experimentally determined current efficiency calculated from both the rate of salt depletion and through the transport number model.

importance of the use of a delayed differential temporal material balance.

The current density can be seen to fall to a non-zero value ($\sim$3 A/m^2, 2.6 % of the initial amount) as the solution conductivity falls to a very low value (0.01 mS/cm, 0.16 % of the initial amount) and the single pass conductivity difference nearly vanishing (0.0014 mS/cm). This can be

explained through having a low current efficiency, calculated to be $\sim$20 % (Fig. 4f). At this point, only 20 % of the current results in a net transfer of salt from the diluate to the concentrate. Approximately 40 % of the current is used to transport salt from the concentrate back to the diluate, effectively cancelling out part of the 60 % of current driving salt in the useful direction. The current efficiency decreases because the

concentrate concentration increases far above that of the diluate, steepening the transmembrane electrochemical potential gradient and the driving force on co-ions in the concentrate. This clearly demonstrates the need for an accurate current efficiency model when large concentration differences are present. The intrinsic transport number provided by manufacturers is above 99 %, which could, seemingly reasonably, lead to the assumption of perfect permselectivity. However, it is clear that this assumption becomes increasingly erroneous throughout the experiment.

The goodness of fit between model and experimental results was quantified using the average absolute difference (AAD) metric:

$$\text{AAD} = \frac{1}{N} \sum_{o=\text{observation}} |\chi_o - \bar{\chi}_o| \qquad (37)$$

Here, N is the total number of data points in an experiment, χ_o is a certain experimentally observed data point, and $\bar{\chi}_o$ is the associated model predicted observation. The AAD values of the experimentally measured quantities are shown in Table 3 alongside the values of each variable at the beginning of the experiment. Excellent agreement between the experimental results and model can be seen, with all AAD values around two orders of magnitude below the initial variable values. These low difference values demonstrate the high accuracy of the model and is significant as no fitting parameters were utilised which would ensure a good fit.

The divergence of a temporal experiment from model predictions are expected to be much larger than with a single steady-state measurement. This is because small errors compound over time, feeding back between the concentration and current density. The greatest sources of error within the experiments stem from control of the volumetric flow rate and the total volume of fluid within each circuit. These are difficult to control accurately and have a large effect on the measured data. Despite best efforts to fix them precisely, it is likely that remaining errors stem principally from these parameters. Nevertheless, the close resemblance of the model and experimental results for all concentrations demonstrates that the model is valid over a range of concentrations and fluxes.

The novel transport number model presented in this work appears to accurately capture both the trend of the current efficiency and the phenomenon driving it. The current efficiency can be found directly from the single pass concentration difference for a stream (ΔC_j) and the current density through the following equation:

$$\phi = \frac{\Delta C_j \, Q_j \, F}{i \, A_m \, n} \qquad (38)$$

Here, A_m is the area of one membrane. The equation expresses the ratio of useful current ($\Delta C \, Q / n \, F$) to total current ($i \, A_m$). This value can be calculated from experimental data and is shown in orange in Fig. 4 f. A similar trend between the model and experimental results is seen for this validation but diverge significantly at later times. It should be noted that the experimental data curves have undergone smoothing using a moving mean method. Towards later times, the solution conductivity approaches the detection limit of the probe, and so the uncertainty increases to over 100 %. Consequently, the data towards the end of the experiment is unreliable. Nevertheless, the qualitative agreement for the current efficiency data and the excellent quantitative agreement for both the current density and conductivities demonstrates that the current

Table 3
Values of the average absolute difference (AAD) between experimental and model values for measured quantities, along with their initial values for temporal experiments.

Measured Variable	AAD	Initial Value
Current Density	2.563 A/m^2	111 A/m^2
Diluate Inlet	0.051 mS/cm	5.95 mS/cm
Diluate Outlet	0.105 mS/cm	5.95 mS/cm
Concentrate Inlet	0.055 mS/cm	5.95 mS/cm
Concentrate Outlet	0.063 mS/cm	5.95 mS/cm

efficiency is accurately captured in the model. However, this is not sufficient to fully validate the transport number model.

The underlying cause of the reduction in current efficiency was assumed to be the increase in the trans-membrane concentration difference. The transport number model may be isolated and independently validated using the measured conductivities. Eq. 32 was used to calculate an experimental transport number for each membrane using the measured conductivities converted into concentrations. These transport numbers are then aggregated into a current efficiency through Eq. 27. The results of this are shown in yellow in Fig. 4f. Excellent agreement is seen with the model for much of the experiment which breaks down towards the end as the uncertainty in the conductivity grows to over 50 %. Overall, Fig. 4f demonstrates that the transport number model accurately describes not just the effect on the current efficiency, but the underlying phenomenon as well. This is crucial because it shows that a simple model which uses only manufacturer data can be used to capture the current efficiency up to extreme concentration differences where the selectivity falls to very low levels.

3.3. Steady-state validation

Current-voltage curves are used prevalently in ED research to determine the limiting current density as well as the ohmic resistance of the stack. These values are essential for process modelling and used to compute the power consumption and membrane area which are vital for cost optimisation. For a given desired outlet concentration and flowrate, the power consumption per unit volume of treated water is proportional to the stack voltage. Conversely, the total membrane area is inversely proportional to the stack voltage. Therefore, an optimum voltage can be found through minimisation of the overall cost. As such, it is important that the model presented herein is valid over all voltages below the LCD.

Fig. 5a shows the controlled voltage and measured current over time for the steady state experiments. After each step increase in voltage, the current experiences a step increase as well, before asymptotically decreasing to a new steady state value. The initial surge of current could potentially be caused by the transient thickening of the electric double layer or increasing concentration polarisation adjacent to the membrane. Additional current would flow to cause these effects which would dissipate over time. As the model presented is not designed to consider these transient migratory behaviours, only the steady state current is used for validation.

The inlet and outlet conductivities of the diluate and concentrate streams over time are shown in Fig. 5b. The inlet concentrations for both the concentrate and diluate streams are constant throughout the experiment, demonstrating that a steady state was achieved using the experimental method described in Section 3.1. The outlet conductivities of the diluate and concentrate are seen to decrease and increase stepwise, respectively. These steps coincide with the step increases in the applied voltage and show a greater amount of salt is removed in a single pass when a higher voltage is applied, as is expected. After the end of the experiment, at ~3500 s, the outlet conductivities fall immediately back to being the same as the inlet conductivities, again demonstrating that an effective steady-state environment has been achieved.

The experimental and model current-voltage curves are shown in Fig. 5c. For low voltages (0-1 V), the current density is zero. This is because the applied voltage is lower than the equilibrium voltage (1.23 V), and without electrode reactions, no current can flow. Above this value, the current-voltage curve is near-linear. A linear relationship is characteristic of an unchanging electric resistance, the calculated values of which can be seen in Fig. 5e. The electrolyte resistance is the only resistive element which changes with the applied voltage. It decreases because despite the inlet salt concentration being constant, a higher voltage results in a greater amount of salt transferred from the diluate in a single pass. This decreases the concentration of the diluate and increases the concentration of the concentrate by the same amount. Since the resistance is inversely proportional to the salt concentration, the
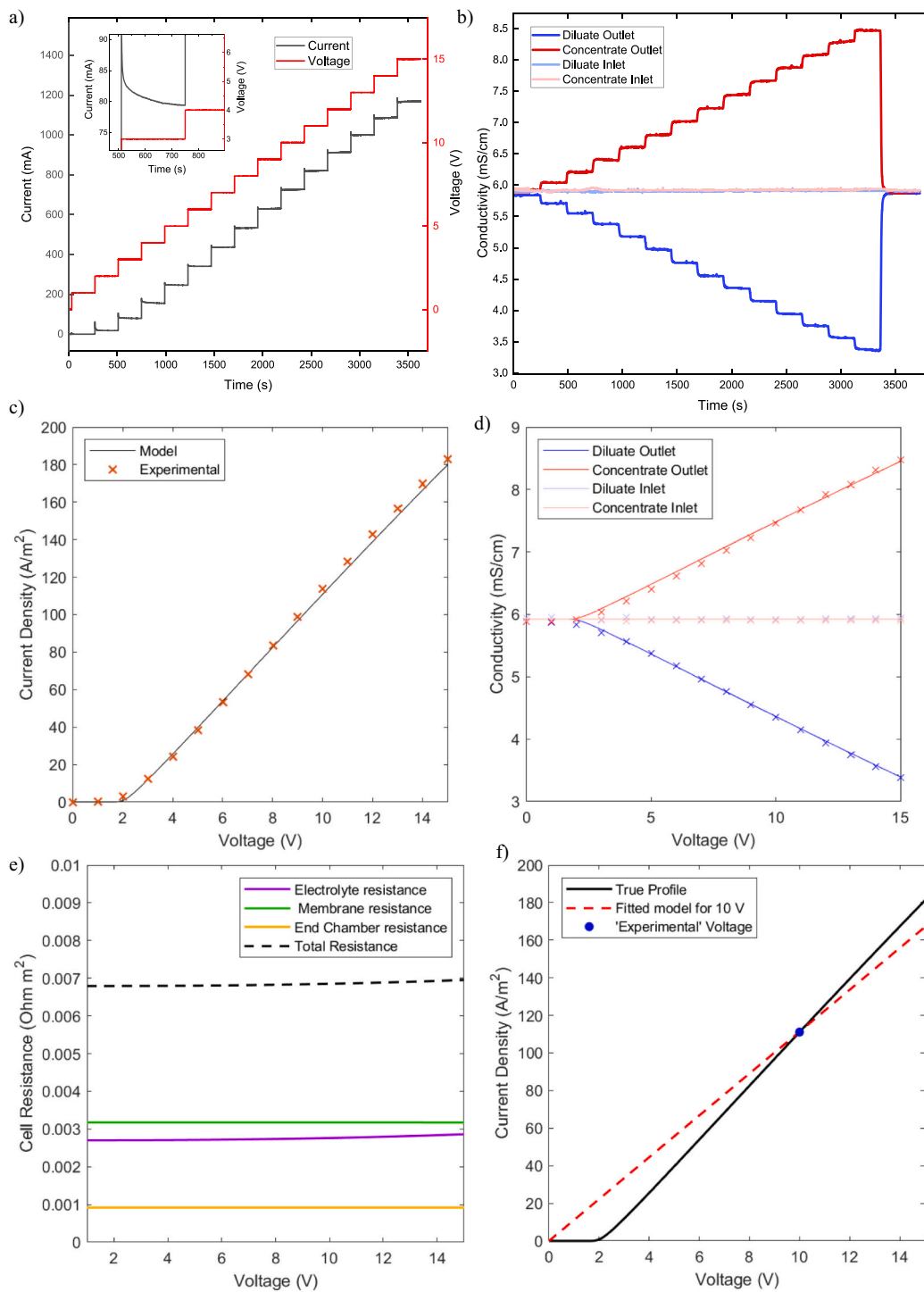
Fig. 5. Figures showing the results of the steady-state validation experiments. a) The temporal evolution of the applied voltage and measured current showing the step increases in voltage and the transient behaviour of the current. b) The temporal evolution of the inlet and outlet conductivities of the diluate and concentrate streams. c) The current voltage curve for both the experimentally measured data (crosses) and model prediction (line). d) The voltage-conductivity plot for experimentally measured data (crosses) and model predictions. e) Variation of the constituents of the resistance of a single cell with the applied voltage. f) A current voltage plot showing the 'true' modelled profile, and a generic model which excludes the overpotential and equilibrium potential, empirically fit to experimental data at 10 V.

increase in the diluate resistance is larger, resulting in an overall increase in resistance. Nevertheless, the outlet diluate concentration only decreases by about 40 % at the highest voltage and so the increase in resistance is very low. This effect is further reduced due to the other fixed contributors to the resistance and the fact that the electrolyte resistance is averaged over the entire path length inside the stack.

The model predicted and experimentally measured conductivities are seen in Fig. 5d. As with the current density, there is no response for voltages below the equilibrium voltage. Above this, the diluate and concentrate decrease and increase linearly with voltage, respectively. At these concentrations, the current efficiency remains relatively constant at above 0.99. As such, over this voltage range the current density and

inlet-outlet salt concentration difference is directly proportional (Eq. 37) and so the outlet conductivity trends are expected to be linear.

As with the temporal validation, the AAD was used to quantify the goodness of fit of the models (Table 4). Once again, excellent agreement is seen between the model and experimental results over the entire range of voltages, shown by AAD values two orders of magnitude below the range of experimental data. Consequently, it is shown that that the model accurately captures ED behaviour over a wide range of voltages. This is vital to ensure that the model is globally valid, and to ensure that ED voltage optimisation will be accurate. Further, it demonstrates that modelling the electrode reactions using the equilibrium potential and overpotential (using the Tafel equation) is necessary for global accuracy. A model without these potentials would only be able to capture a single temporal experiment using a resistance fitting parameter, and the equivalent current-voltage curve would be a straight line through the origin (Fig. 5f). Although this method would suffice for one design at a single voltage, it is apparent that at all other voltages, the model would not be accurate. Optimising the voltage is a key aspect of the design of all electromembrane processes, and so accurately capturing the behaviour over a wide range of voltages is paramount.

The membrane resistance hardly increases over both time the temporal experiments (Fig. 4f) and voltage in the steady-state experiments (Fig. 5e). This is primarily due to the low range of concentrations that are present in the validation experiments, chosen to ensure that the current and voltage were well below the upper detection limits of the potentiostat (2 A, 30 V) and that the LCD was not reached. The low NaCl concentrations result in a high electrolyte resistance relative to the membrane resistance. The impact of the membrane resistance at a wider range of concentrations is evaluated in Section 4.

4. Exploration of novel model aspects

The model presented herein contains several novel aspects, most notably the membrane resistance model and transport number model. In this section, the impact of these two aspects is investigated for their impact on the modelling results.

The full details of the membrane resistance model can be found in a recent publication by Fan et al. [61]. Typically, membrane electrical resistances are considered constant in ED models, but realistically it varies with the salt identity and its concentration in the concentrate and diluate streams. Membrane resistances are often provided by manufacturers, but these will be only valid for a certain salt and concentration (typically 1 M NaCl). Membrane resistance can be accurately measured experimentally through electrochemical impedance spectroscopy (EIS) using a potentiostat [70]. However, this will still only be valid at that experimental concentration. The method presented by Fan et al. (Eqs. 11–17) allows the membrane resistance to be modelled as a function of the external solution identity and concentration. Furthermore, the membrane model has been validated for bivalent and trivalent ions, ensuring that the electromembrane modelling strategy presented herein has global applicability across a range of salts and concentrations.

Fig. 6a shows how the membrane electrical resistance varies with NaCl solution concentration. The membrane resistance is relatively constant at very low solution concentration, but decreases by an order of
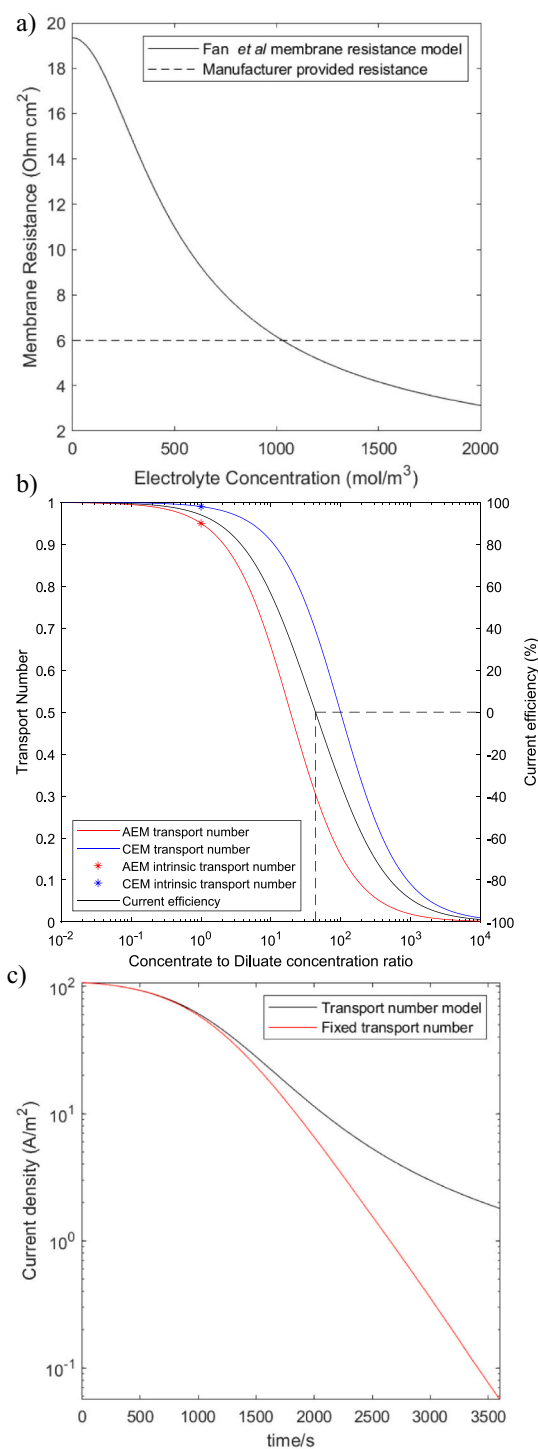
Table 4
Values of the average absolute difference (AAD) between experimental and model values for measured quantities for steady-state experiments.

Measured Variable	AAD
Current Density	1.956 A/m^2
Diluate Inlet	0.020 mS/cm
Diluate Outlet	0.024 mS/cm
Concentrate Inlet	0.009 mS/cm
Concentrate Outlet	0.045 mS/cm

Fig. 6. a) A graph of how the membrane resistance changes with the electrolyte concentration as well as the resistance provided by the membrane manufacturer. b) Results of how the transport number model (left y-axis, Eq. 32) and current efficiency (right y-axis, Eq. 27) vary with the ratio of the concentration of the concentrate to the diluate. Also shown are the intrinsic transport numbers provided by the membrane manufacturer and the maximum separation ratio. c) time evolution of the calculated current density with a transport number fixed at the intrinsic value and the with a varying transport number.

magnitude as the electrolyte concentration increases from zero to 2 mol/L. This is because at low concentrations, the internal membrane counterion concentration is almost equal to the membrane fixed charge density and the co-ion concentration is negligible. However, as the

external solution concentration increases, the solution concentration inside the membrane pores increases, resulting in an increase of the conductivity(Eq. 15). As the external solution concentration approaches the range of the fixed charge density, co-ions become significant charge carriers, further reducing the resistance. This demonstrates why an advanced membrane resistance model which varies with electrolyte identity and concentration is important for model globality. The membrane resistance provided by the manufacturer (6 Ω cm^2) intersects the curve at around 1 mol/L, which is likely to be the conditions at which the resistance was measured.

Membrane transport numbers are also provided by membrane manufacturers and are considered constant in most ED models. The transport numbers for each membrane in the model presented herein are a function of the transmembrane concentration difference (Eq. 28). Fig. 6b shows how the transport numbers for each of the membranes varies with the transmembrane concentration ratio (concentrate to diluate), along with the intrinsic transport numbers and current efficiency. Transport numbers are equal to the intrinsic transport number when the concentration ratio is one (by definition). At concentration ratios lower than this, the transport numbers and current efficiency tend to unity as counterion transport dominates. At higher concentration ratios, the transport numbers decrease and asymptotically tend to zero. The current efficiency tends to negative one as co-ion transport dominates. The current efficiency is zero when the concentration ratio is about 42. This represents an equilibrium where the flux of counterions and co-ions are equal, resulting in no overall transfer between the concentrate and diluate. As such, this is the effective separation limit for the ED stack. It is dependent only on the intrinsic transport numbers of the membranes and can be calculated by the following equation.

$$\left(\frac{C_c}{C_d}\right)_{max} = \frac{1}{\sqrt{\left(\frac{1}{t_{0,aem}} - 1\right)\left(\frac{1}{t_{0,cem}} - 1\right)}} \tag{39}$$

This equation is derived by combining Eqs. 32 and 27 and setting ϕ equal to zero. The importance of membrane selectivity on high degrees of separation is made apparent through this equation. Further, the maximum concentration ratio serves as an important design parameter as it would instruct what degree of separation would be attainable.

Fig. 6c shows a comparison of the temporal evolution of the current density when the transport numbers are fixed at the values provided by the membrane manufacturer and vary with the concentration as per Eq. 32. Initially, the current densities are very similar as the concentration ratio is close to one, and thus the transport numbers are close to their intrinsic values. However, the current density in the fixed transport number model drops to a very low value much faster than in the varied transport number model due to the much higher current efficiency when there is a large transmembrane concentration difference. The difference in these values at the end of the time series would result in an underprediction of the power consumption by a factor of 32 if fixed transport numbers were used. As with the membrane resistance model, this demonstrates how crucial a transport number model is for model globality over a range of concentrations.

5. Conclusion

A robust layered circuit-based model of conventional ED is presented herein, the fundamental strategies of which may be applied to a wide range of electromembrane processes. The innermost layer of the model uses Ohm's law to compute the current density within a differential volume tangent to the direction of flow for a given cell electrical resistance. This is passed to the middle layer which converts the current density into a flux through the Faraday constant and current efficiency, which is then integrated to generate a spatial concentration profile. At this point, key variables for process design and optimisation including outlet concentration, overall current density, and power consumption can be extracted. An outer layer utilises a time-delayed differential material balance to compute how reservoirs in a recirculating batch system vary over time while accounting for the pipe dead time, which can be significant in laboratory systems.

This model was validated on a standard recirculating batch experiment and through how the steady-state behaviour varies with applied voltage. Both methods showed excellent agreement between model results and experimental data, with values of the average absolute difference being two orders of magnitude below the range of values measured. This is noteworthy since no parameter fitting was conducted. Further, it demonstrates that the model is valid over a wide range of concentrations and voltages and has not been undermined by confounding phenomena.

To ensure model globality, a membrane resistance model and novel transport number model have been utilised. These were shown to have a significant impact on the model behaviour and were crucial to accurately capture ED behaviour over a wide range of salts and concentrations. The impact of the transport number model was found to be particularly strong when the diluate concentration is far lower than the concentrate concentration, as this leads to a very low current efficiency resulting from excessive back-migration. The membrane resistance model was found to be more impactful when the overall concentration varies over multiple orders of magnitude. Although the membrane resistance may not have a significant impact over a single batch experiment, it is important for extending the results to processes with different concentrations or different salts.

The modelling strategy presented is inherently flexible due to the presence of the multiple layers and analogy to an electrical circuit. As such, additional features can be added to the model with ease through modifications to the material balance and the consideration of auxiliary resistive elements. Examples of process units which can be modelled using this strategy include bipolar membrane electrodialysis, electrodialysis metathesis, electrodeionisation, and electromembrane reactors. Kinetic or equilibrium contributions to the material balance can account for any reactions present which is vital for BPMED. Membrane fouling can also be accounted for through an additional electrical resistance term. Concentration gradients within boundary layers can be considered using mass transport coefficients and Sherwood number correlations. This will be particularly impactful for low concentration ED and may be taken further to model behaviour of ED at or above the LCD by accounting for the potential drop over a space charge region and the mixing resulting from electroconvection. This is becoming ever more important as industrial operation of ED at overlimiting conditions is explored.

Membranes were characterised in the model through only their thickness, fixed charge concentration, and intrinsic transport number (when the transmembrane salt concentrations are equal). These are all fixed fundamental properties of a membrane which are either provided by membrane manufacturers or can be measured through simple experiments. Consequently, they will remain fixed as process conditions change and thus the models should be globally valid. As such, an ideal membrane may be chosen for a given application through optimisation using this model.

Fundamentally, this model was designed to contain no empirical parameters and be globally valid. Further, the model is applicable to both a recirculating batch system and a steady-state continuous process. As such, any model developed with this strategy may be validated on laboratory-scale batch system and then used in process modelling software for full scale design and optimisation. Therefore, this represents a powerful tool for both researchers and industrial electromembrane process designers.

Nomenclature

Latin symbol

AAD	average absolute difference
A	membrane physical parameter collection
A_a A_c	Tafel slope parameters
A_m	area of one membrane
C	concentration
C_{fix}	membrane fixed charge concentration
d	distance
D	diffusivity
e	elementary charge
F	Faraday constant
f_w	membrane water volume fraction
i	current density
$i_{0,a}$ $i_{0,c}$	Tafel exchange current density parameter
J	ion flux
k_B	Boltzmann's constant
n	number of repeating cells
N	total number of experimental data points
N_A	Avogadro's constant
Q	volumetric flow rate
R	electric resistance
R_g	gas constant
t	time
$\bar{t}$	transport number
$\boldsymbol{u}$	velocity
u_c	channel velocity
V_{cell}	cell voltage
V_{ec}	end chamber voltage drop
V_{eq}	equilibrium Voltage
V_{stack}	stack voltage
x	spatial coordinate
y	distance coordinate through the membrane
z	ion charge number

Greek symbol

ε_0	permittivity of free space
ε_r	relative permittivity
Φ	electric potential
γ	activity coefficient
η	Overpotential
θ	coefficient of the summation of infinite vectors
κ	conductivity
μ	ion mobility
ν	ion stoichiometry
τ	time delay
ϕ	current efficiency
χ	experimentally measured data point
$\bar{\chi}$	model predicted data point

Subscript

0	referring to conditions when the concentrate and diluate are of equal concentration
AEM	anion exchange membrane
C	concentrate
an	anion
ca	cation
co	*Co*-ion
ct	counterion
CEM	cation exchange membrane
D	diluate
ec	referring to the end chamber domain
ex	referring to the stack exit conditions
i	ion species
j ($= C, D$)	solution channel
m ($= CEM, AEM$)	membrane
o	observation
R	referring to reservoir domain
s	solution

Supplementary data to this article can be found online at https://doi.org/10.1016/j.desal.2024.117386.

Declaration of competing interest

The authors declare the following financial interests/personal relationships which may be considered as potential competing interests:

Jack Ledingham reports financial support was provided by the Engineering and Physical Sciences Research Council. Jack Ledingham reports financial support was provided by Shell Global Solutions International BV. Kyra Sedransk Campbell reports financial support was provided by the Royal Society. If there are other authors, they declare that they have no known competing financial interests or personal relationships that could have appeared to influence the work reported in this paper.

Data availability

Data will be made available on request.

References

[1] UNESCO, Valuing water - The United Nations World Water Development Report 2021, Water Politics 206, 2021. https://unesdoc.unesco.org/ark:/48223/pf0000375724 (accessed July 16, 2021).

[2] A. Boretti, L. Rosa, Reassessing the projections of the world water development report, Nature Clean Water (2019), https://doi.org/10.1038/s41545-019-0039-9.

[3] United Nations, The United Nations world water development report 2020: water and climate change - UNESCO Digital Library. https://unesdoc.unesco.org/ark:/48223/pf0000372985.locale=en, 2020 (accessed February 19, 2021).

[4] UN, The United Nations World Water Development Report 2023: Partnerships and cooperation for water. https://unesdoc.unesco.org/ark:/48223/pf0000384655, 2023 (accessed June 27, 2023).

[5] H. Fan, Y. Huang, N.Y. Yip, Advancing ion-exchange membranes to ion-selective membranes: principles, status, and opportunities, Frontiers of Environmental Science & Engineering 17 (2) (2023) 1–27, https://doi.org/10.1007/S11783-023-1625-0, 17 (2022).

[6] S. Al-Amshawee, M.Y.B.M. Yunus, A.A.M. Azoddein, D.G. Hassell, I.H. Dakhil, H. A. Hasan, Electrodialysis desalination for water and wastewater: a review, Chem. Eng. J. 380 (2020) 122231, https://doi.org/10.1016/j.cej.2019.122231.

[7] B. Chen, Z. Zhang, C. Jiang, R. Fu, J. Yan, H. Wang, R. Li, G. Cao, Y. Wang, T. Xu, Electro-membrane reactor: a powerful tool for green chemical engineering, AICHE J. 69 (2023) e18140, https://doi.org/10.1002/AIC.18140.

[8] J. Xu, G. Zhong, M. Li, D. Zhao, Y. Sun, X. Hu, J. Sun, X. Li, W. Zhu, M. Li, Z. Zhang, Y. Zhang, L. Zhao, C. Zheng, X. Sun, Review on electrochemical carbon dioxide capture and transformation with bipolar membranes, Chin. Chem. Lett. 34 (2023) 108075, https://doi.org/10.1016/j.CCLET.2022.108075.

[9] C.M. Liang, C.C. Wang, K.J. Huang, C.F. Yang, Production of biohydrogen and green platform compound 2, 5-furandicarboxylic acid using rice straw hydrolysate, Biochem. Eng. J. 197 (2023) 108993, https://doi.org/10.1016/J.BEJ.2023.108993.

[10] Y. Liu, M. Lv, X. Wu, J. Ding, L. Dai, H. Xue, X. Ye, R. Chen, R. Ding, J. Liu, B. Van der Bruggen, Recovery of copper from electroplating sludge using integrated bipolar membrane electrodialysis and electrodeposition, J. Colloid Interface Sci. 642 (2023) 29–40, https://doi.org/10.1016/J.JCIS.2023.03.154.

[11] Y. Zhang, Z. Zhang, K. Guo, X. Liang, Controllable recovery and recycling of carboxylic acid-polyalcohol deep eutectic solvent for biomass pretreatment with electronically-controlled chemical methodology, Bioresour. Technol. 365 (2022) 128175, https://doi.org/10.1016/J.BIORTECH.2022.128175.

[12] Y. Liu, Y. Sun, Z. Peng, Evaluation of bipolar membrane electrodialysis for desalination of simulated salicylic acid wastewater, Desalination 537 (2022) 115866, https://doi.org/10.1016/J.DESAL.2022.115866.

[13] Y. Zhao, X. Wang, J. Yuan, Z. Ji, J. Liu, S. Wang, X. Guo, F. Li, J. Wang, J. Bi, An efficient electrodialysis metathesis route to recover concentrated NaOH-NH4Cl products from simulated ammonia and saline wastewater in coal chemical industry, Sep. Purif. Technol. 301 (2022), https://doi.org/10.1016/j.seppur.2022.122042.

[14] H. Jaroszek, A. Lis, P. Dydo, Transport of impurities and water during potassium nitrate synthesis by electrodialysis metathesis, Sep. Purif. Technol. 158 (2016) 87–93, https://doi.org/10.1016/J.SEPPUR.2015.12.009.

[15] K. Haerens, P. De Vreese, E. Matthijs, L. Pinoy, K. Binnemans, B. Van Der Bruggen, Production of ionic liquids by electrodialysis, Sep. Purif. Technol. 97 (2012) 90–95, https://doi.org/10.1016/J.SEPPUR.2012.02.017.

[16] P.F. Li, Q.B. Chen, J. Wang, Y. Xu, L. Dong, J. Wang, Developing a reclamation strategy for softening nanofiltration brine: a scaling-free conversion approach via continuous two-stage electrodialysis metathesis, Sci. Total Environ. 807 (2022) 150374, https://doi.org/10.1016/J.SCITOTENV.2021.150374.

[17] A. Saravanan, P.R. Yaashikaa, P. Senthil Kumar, S. Karishma, P. Thamarai, V.C. Deivayanai, G. Rangasamy, R. Selvasembian, T.M. Aminabhavi, Environmental sustainability of toxic arsenic ions removal from wastewater using electrodeionization, Sep. Purif. Technol. 317 (2023) 123897, https://doi.org/10.1016/J.SEPPUR.2023.123897.

[18] C. Otero, A. Urbina, E.P. Rivero, F.A. Rodríguez, Desalination of brackish water by electrodeionization: experimental study and mathematical modeling, Desalination 504 (2021) 114803, https://doi.org/10.1016/J.DESAL.2020.114803.

[19] E.N. Sarıçiçek, M.M. Tuğaç, V.T. Özdemir, İ.Y. İpek, Ö. Arar, Removal of boron by boron selective resin-filled electrodeionization, Environ. Technol. Innov. 23 (2021) 101742, https://doi.org/10.1016/J.ETI.2021.101742.

[20] H. Julian, K. Khoiruddin, N. Julies, V. Edwina, I.G. Wenten, Pineapple juice acidity removal using electrodeionization (EDI), J. Food Eng. 304 (2021) 110595, https://doi.org/10.1016/J.JFOODENG.2021.110595.

[21] D. Babilas, P. Dydo, Selective zinc recovery from electroplating wastewaters by electrodialysis enhanced with complex formation, Sep. Purif. Technol. 192 (2018) 419–428, https://doi.org/10.1016/j.seppur.2017.10.013.

[22] C. Jiang, H. Chen, Y. Zhang, H. Feng, M.A. Shehzad, Y. Wang, T. Xu, Complexation Electrodialysis as a general method to simultaneously treat wastewaters with metal and organic matter, Chem. Eng. J. 348 (2018) 952–959, https://doi.org/10.1016/j.cej.2018.05.022.

[23] Z. Liu, D. Lu, H. Guo, J. Zhang, S. Tao, R. Chen, L.Y. Chen, M. Gong, Experimental study and prospect analysis of LiBr-H2O reverse electrodialysis heat engine, Appl. Energy 350 (2023) 121791, https://doi.org/10.1016/J.APENERGY.2023.121791.

[24] G. Campisi, A. Cosenza, F. Giacalone, S. Randazzo, A. Tamburini, G. Micale, Desalination of oilfield produced waters via reverse electrodialysis: a techno-economical assessment, Desalination 548 (2023) 116289, https://doi.org/10.1016/J.DESAL.2022.116289.

[25] C. Simões, B. Vital, T. Sleutels, M. Saakes, W. Brilman, Scaled-up multistage reverse electrodialysis pilot study with natural waters, Chem. Eng. J. 450 (2022) 138412, https://doi.org/10.1016/j.cej.2022.138412.

[26] M.A. Maluleke, V.M. Linkov, Partial electrochemical oxidation of phenol on ceramic-based flat-sheet type electromembrane reactors, Sep. Purif. Technol. 32 (2003) 377–385, https://doi.org/10.1016/S1383-5866(03)00065-0.

[27] F. Karimi, S.N. Ashrafizadeh, F. Mohammadi, Process parameter impacts on adiponitrile current efficiency and cell voltage of an electromembrane reactor using emulsion-type catholyte, Chem. Eng. J. 183 (2012) 402–407, https://doi.org/10.1016/J.CEJ.2011.12.031.

[28] M.T. Demeuse, Production and applications of hollow fibers, Handbook of Textile Fibre Structure 2 (2009) 485–499, https://doi.org/10.1533/9781845697310.3.485.

[29] J. Ledingham, K.L. Sedransk Campbell, B. In 't Veen, L. Keyzer, A.N. Campbell, Barriers to electrodialysis implementation: maldistribution and its impact on resistance and limiting current density, Desalination 531 (2022) 115691, https://doi.org/10.1016/J.DESAL.2022.115691.

[30] H. Zhu, B. Yang, C. Gao, Y. Wu, Ion transfer modeling based on Nernst–Planck theory for saline water desalination during electrodialysis process, Asia Pac. J. Chem. Eng. 15 (2020), https://doi.org/10.1002/apj.2410.

[31] S. Casas, N. Bonet, C. Aladjem, J.L. Cortina, E. Larrotcha, L.V. Cremades, Modelling sodium chloride concentration from seawater reverse osmosis brine by electrodialysis: preliminary results, Solvent Extr. Ion Exch. 29 (2011) 488–508, https://doi.org/10.1080/07366299.2011.573451.

[32] A. Ghorbani, A. Ghassemi, Brackish Water Desalination Using Electrodialysis: Predictive Mass Transfer and Concentration Distribution Model Along the Electrodialyzer (2018), https://doi.org/10.2166/wst.2017.547.

[33] K. Tado, F. Sakai, Y. Sano, A. Nakayama, An analysis on ion transport process in electrodialysis desalination, Desalination 378 (2016) 60–66, https://doi.org/10.1016/j.desal.2015.10.001.

[34] A.H. Galama, G. Daubaras, O.S. Burheim, H.H.M. Rijnaarts, J.W. Post, Seawater electrodialysis with preferential removal of divalent ions, J. Membr. Sci. 452 (2014) 219–228, https://doi.org/10.1016/j.memsci.2013.10.050.

[35] M. Tedesco, H.V.M. Hamelers, P.M. Biesheuvel, Nernst-Planck transport theory for (reverse) electrodialysis: I, Effect of co-ion transport through the membranes, J Memb Sci 510 (2016) 370–381, https://doi.org/10.1016/j.memsci.2016.03.012.

[36] R. Kodým, P. Pánek, D. Šnita, D. Tvrzník, K. Bouzek, Macrohomogeneous approach to a two-dimensional mathematical model of an industrial-scale electrodialysis unit, J. Appl. Electrochem. 42 (2012) 645–666, https://doi.org/10.1007/s10800-012-0457-6.

[37] F. Scholz, Books on fundamental electrochemistry and electroanalytical techniques, Electroanalytical Methods (2010) 343–345, https://doi.org/10.1007/978-3-642-02915-8_19.

[38] Mémoire Poisson, sur la théorie du magnétisme en mouvement, Mémoires de l'Académie Royale Des Sciences de l'Institut de France (1823) 441–570.

[39] M.K. Urtenov, A.M. Uzdenova, A.V. Kovalenko, V.V. Nikonenko, N.D. Pismenskaya, V.I. Vasil'eva, P. Sistat, G. Pourcelly, Basic mathematical model of overlimiting transfer enhanced by electroconvection in flow-through electrodialysis membrane cells, J. Membr. Sci. 447 (2013) 190–202, https://doi.org/10.1016/J.MEMSCI.2013.07.033.

[40] J. Kaláb, Z. Palatý, Electrodialysis of tartaric acid: batch process modelling, Separation Science and Technology (Philadelphia) 47 (2012) 2262–2272, https://doi.org/10.1080/01496395.2012.673042.

[41] Y. Guo, A. Al-Jubainawi, Z. Ma, Mathematical modelling and simulation analysis of electrodialysis regeneration for LiCl liquid desiccant air conditioning systems, Int. J. Refrig. 107 (2019) 234–245, https://doi.org/10.1016/j.ijrefrig.2019.08.006.

[42] B. Sun, M. Zhang, S. Huang, J. Wang, X. Zhang, Limiting concentration during batch electrodialysis process for concentrating high salinity solutions: a theoretical and experimental study, Desalination 498 (2021) 114793, https://doi.org/10.1016/j.desal.2020.114793.

[43] M.B.S. Ali, B. Hamrouni, Development of a predictive model of the limiting current density of an electrodialysis process using response surface methodology, Membrane Water Treatment 7 (2016) 127–141, https://doi.org/10.12989/mwt.2016.7.2.127.

[44] S. Pawlowski, C.F. Galinha, J.G. Crespo, S. Velizarov, Prediction of reverse electrodialysis performance by inclusion of 2D fluorescence spectroscopy data into multivariate statistical models, Sep. Purif. Technol. 150 (2015) 159–169, https://doi.org/10.1016/j.seppur.2015.06.032.

[45] G. Grossman, A.A. Sonin, Membrane fouling in electrodialysis: a model and experiments, Desalination 12 (1973) 107–125, https://doi.org/10.1016/S0011-9164(00)80178-2.

[46] W. Kujawski, A. Yaroshchuk, E. Zholkovskiy, I. Koter, S. Koter, Analysis of membrane transport equations for reverse electrodialysis (red) using irreversible thermodynamics, Int. J. Mol. Sci. 21 (2020) 1–13, https://doi.org/10.3390/ijms21176325.

[47] Y. Xiang Jia, F. Jiao Li, X. Chen, M. Wang, Model analysis on electrodialysis for inorganic acid recovery and its experimental validation, Sep. Purif. Technol. 190 (2018) 261–267, https://doi.org/10.1016/j.seppur.2017.08.067.

[48] N.C. Wright, S.R. Shah, S.E. Amrose, A.G. Winter, A robust model of brackish water electrodialysis desalination with experimental comparison at different size scales, Desalination 443 (2018) 27–43, https://doi.org/10.1016/j.desal.2018.04.018.

[49] J.M. Ortiz, J.A. Sotoca, E. Expósito, F. Gallud, V. García-García, V. Montiel, A. Aldaz, Brackish water desalination by electrodialysis: batch recirculation operation modeling, J. Membr. Sci. 252 (2005) 65–75, https://doi.org/10.1016/j.memsci.2004.11.021.

[50] A. Campione, A. Cipollina, I.D.L. Bogle, L. Gurreri, A. Tamburini, M. Tedesco, G. Micale, A hierarchical model for novel schemes of electrodialysis desalination, Desalination 465 (2019) 79–93, https://doi.org/10.1016/j.desal.2019.04.020.

[51] A. Luiz, D.D. McClure, K. Lim, H.G.L. Coster, G.W. Barton, J.M. Kavanagh, Towards a model for the electrodialysis of bio-refinery streams, J. Membr. Sci. 573 (2019) 320–332, https://doi.org/10.1016/j.memsci.2018.11.047.

[52] H.J. Lee, F. Sarfert, H. Strathmann, S.H. Moon, Designing of an electrodialysis desalination plant, Desalination 142 (2002) 267–286, https://doi.org/10.1016/S0011-9164(02)00208-4.

[53] M. Sadrzadeh, A. Kaviani, T. Mohammadi, Mathematical modeling of desalination by electrodialysis, Desalination 206 (2007) 538–546, https://doi.org/10.1016/j.desal.2006.04.062.

[54] B.A. Qureshi, N.A.A. Qasem, S.M. Zubair, Normalized sensitivity analysis of electrodialysis desalination plants for mitigating hypersalinity, Sep. Purif. Technol. 257 (2021), https://doi.org/10.1016/j.seppur.2020.117858.

[55] N.A.A. Qasem, B.A. Qureshi, S.M. Zubair, Improvement in design of electrodialysis desalination plants by considering the Donnan potential, Desalination 441 (2018) 62–76, https://doi.org/10.1016/j.desal.2018.04.023.

[56] H. Nafaa, M. Farhat, S. Lassaad, Mathematical model study of solar electrodialysis desalination, in: in: 2017 International Conference on Electrical and Computing Technologies and Applications, ICECTA 2017, Institute of Electrical and

Electronics Engineers Inc., 2017, pp. 1–4, https://doi.org/10.1109/ICECTA.2017.8251946.

[57] M. Fidaleo, M. Moresi, Optimal strategy to model the electrodialytic recovery of a strong electrolyte, J. Membr. Sci. 260 (2005) 90–111, https://doi.org/10.1016/j.memsci.2005.01.048.

[58] N.C. Wright, S.R. Shah, S.E. Amrose, A.G. Winter, A robust model of brackish water electrodialysis desalination with experimental comparison at different size scales, Desalination 443 (2018) 27–43, https://doi.org/10.1016/j.desal.2018.04.018.

[59] K.G. Nayar, P. Sundararaman, C.L. O'Connor, J.D. Schacherl, M.L. Heath, M. O. Gabriel, S.R. Shah, N.C. Wright, A.G. Winter V, Feasibility study of an electrodialysis system for in-home water desalination in urban India, Dev Eng 2 (2017) 38–46, https://doi.org/10.1016/J.DEVENG.2016.12.001.

[60] A. Campione, L. Gurreri, M. Ciofalo, G. Micale, A. Tamburini, A. Cipollina, Electrodialysis for water desalination: a critical assessment of recent developments on process fundamentals, models and applications, Desalination 434 (2018) 121–160, https://doi.org/10.1016/j.desal.2017.12.044.

[61] H. Fan, Y. Huang, I.H. Billinge, S.M. Bannon, G.M. Geise, N.Y. Yip, Counterion mobility in ion-exchange membranes: spatial effect and valency-dependent electrostatic interaction, ACS ES and T Engineering 2 (2022) 1274–1286, https://doi.org/10.1021/acsestengg.1c00457.

[62] S. Ozkul, J.J. van Daal, N.J.M. Kuipers, R.J.M. Bisselink, H. Bruning, J.E. Dykstra, H.H.M. Rijnaarts, Transport mechanisms in electrodialysis: the effect on selective ion transport in multi-ionic solutions, J. Membr. Sci. 665 (2023), https://doi.org/10.1016/j.memsci.2022.121114.

[63] Julius Tafel, Über die Polarisation bei kathodischer Wasserstoffentwicklung, Z. Phys. Chem. 50 (1905) 641–712.

[64] A. Einstein, Über die von der molekularkinetischen Theorie der Wärme geforderte Bewegung von in ruhenden Flüssigkeiten suspendierten Teilchen, Ann. Phys. 322 (1905) 549–560.

[65] M. von Smoluchowski, Zur kinetischen Theorie der Brownschen Molekularbewegung und der Suspensionen, Ann. Phys. 326 (1906) 756–780.

[66] P. Fievet, Donnan effect, in: Encyclopedia of Membranes, Springer, Berlin Heidelberg, 2014, pp. 1–3, https://doi.org/10.1007/978-3-642-40872-4_1714-1.

[67] J. Veerman, J.W. Post, M. Saakes, S.J. Metz, G.J. Harmsen, Reducing power losses caused by ionic shortcut currents in reverse electrodialysis stacks by a validated model, J. Membr. Sci. 310 (2008) 418–430, https://doi.org/10.1016/j.memsci.2007.11.032.

[68] A. Culcasi, L. Gurreri, A. Zaffora, A. Cosenza, A. Tamburini, A. Cipollina, G. Micale, Ionic shortcut currents via manifolds in reverse electrodialysis stacks, Desalination 485 (2020), https://doi.org/10.1016/j.desal.2020.114450.

[69] J. Nielsen, A. Adamson, J. Cobble, The Self-diffusion Coefficients of the Ions in Aqueous Sodium Chloride and Sodium Sulfate at 25°, 1952.

[70] A.A. Moya, Electrochemical Impedance of Ion-exchange Membranes With Interfacial Charge Transfer Resistances (2016), https://doi.org/10.1021/acs.jpcc.5b12087.